FLEXURAL PERFORMANCE OF FRP-REINFORCED CONCRETE BEAMS USING ULTRA HIGH STRENGTH CONCRETE

by

Zin Subhi Mahaini

A Thesis presented to the Faculty of the
American University of Sharjah
College of Engineering
In Partial Fulfilment
of the Requirements
for the Degree of

Master of Science in
Civil Engineering

Sharjah, United Arab Emirates

April 2022

Declaration of Authorship

I declare that this thesis is my own work and, to the best of my knowledge and belief, it does not contain material published or written by a third party, except where permission has been obtained and/or appropriately cited through full and accurate referencing.

Signed…… Zin Subhi Mahaini…….

Date……13/04/2022……

Approval Signatures

We, the undersigned, approve the Master's Thesis of Zin Subhi Mahaini

Title: Flexural Performance of FRP-Reinforced Concrete Beams Using Ultra High Strength Concrete

Date of Defense: 13/04/2022

Name, Title and Affiliation	**Signature**
Dr. Farid Abed Professor, Department of Civil Engineering Thesis Advisor	
Dr. Rami Hawileh Professor, Department of Civil Engineering Thesis Committee Member	
Dr. Wael Abuzaid Associate Professor, Department of Mechanical Engineering Thesis Committee Member	
Dr. Irtishad U. Ahmad Head Department of Civil Engineering	
Dr. Lotfi Romdhane Associate Dean College of Engineering	
Dr. Fadi Aloul Dean College of Engineering	
Dr. Mohamed El-Tarhuni Vice Provost for Research and Graduate Studies Office of Research and Graduate Studies	

Acknowledgements

First, I would like to express my deep appreciation and gratitude to my advisor, Dr. Farid Abed, for his constant support and guidance. I would also like to thank my thesis committee members, Dr. Rami Hawileh and Dr. Wael Abuzaid, for their invaluable remarks. Special thanks to the Department of Civil Engineering at the American University of Sharjah for rewarding me with the Graduate Assistantship to complete my master's degree. I am also extremely grateful to Mr. Yazan Alhoubi and Mr. Mohammed Ansari for helping me in conducting the tests in the lab.

Dedication

To my family and friends…

Abstract

This research investigated the flexural performance of beams reinforced with fiber reinforced polymer (FRP) bars and cast using Ultra High Strength Concrete (UHSC) with a nominal compressive strength of 140 MPa. A total of fifteen beams were prepared and tested in a four-point loading setup. Ten specimens were reinforced with Glass FRP (GFRP) bars and two specimens were reinforced with Basalt FRP (BFRP) bars. The other three beams were reinforced with conventional steel as reference specimens. The FRP reinforced beams were designed to have either tension-controlled or compression-controlled modes of failure to examine the different responses between them. All beams had 185 mm width, 250 mm depth, and 2200 mm total span length. The influence of different variables including reinforcement ratio, number of longitudinal bars, and reinforcement type was investigated in terms of strain values, midspan deflections, flexural capacities, and cracking responses. The test results showed that the over-reinforced FRP-UHSC beams displayed acceptable deflections at service loads and had adequate ductility prior to failure. Results also showed that the use of GFRP bars in UHSC beams increased the flexural capacity up to 70.15% compared to steel reinforced beams. The BFRP bars were also found to be valuable alternatives to GFRP bars in flexural members. In addition, the analytical predictions compared well with the experimental values of cracking moments and flexural capacities. However, the ACI 440 and CAN/CSA S806 approaches for calculating midspan deflections underestimated the deflections, especially for over-reinforced FRP-UHSC beams.

Keywords: GFRP; BFRP; Ultra High Strength Concrete; Flexure; Deflection.

Table of Contents

List of Figures

List of Tables

List of Abbreviations

ACI	American Concrete Institute
AFRP	Aramid Fiber Reinforced Polymer
BFRP	Basalt Fiber Reinforced Polymer
CFRP	Carbon Fiber Reinforced Polymer
CSA	Canadian Standards Association
FRC	Fiber Reinforced Concrete
FRP	Fiber Reinforced Polymer
GFRP	Glass Fiber Reinforced Polymer
HPFRCC	High-Performance Fiber-Reinforced Cementitious Composite
HSC	High Strength Concrete
MRI	Magnetic Resonance Imaging
NSC	Normal Strength Concrete
PVA	Polyvinyl Alcohol
RC	Reinforced Concrete
UHPFRC	Ultra-High Performance Fiber Reinforced Concrete
UHSC	Ultra High Strength Concrete

Chapter 1. Introduction

1.1. Introduction

This chapter provides a brief introduction on the Fiber Reinforced Polymer (FRP) bars. It also discusses the properties of the Ultra High Strength Concrete (UHSC) composite material. Then, the chapter presents the problem investigated, the research objectives, and the research significance. Finally, the chapter concludes with the general outline of the thesis.

1.2. Overview

Premature deterioration of concrete structures due to the corrosion of steel reinforcement remains a major problem affecting the construction industry. Steel corrosion can have severe impacts on structural safety, as well as can lead to tremendous economic losses. Therefore, new methods have been employed to tackle the corrosion problem. In recent decades, Fiber Reinforced Polymer (FRP) bars have emerged as a potential alternative to steel reinforcement. Their non-corrosive nature makes them particularly attractive as reinforcement in marine and coastal structures as well as bridges and dams. Other benefits of FRP include their high tensile strength and lightweight. In addition, some FRP materials have unique attractive properties. For example, the Glass FRP (GFRP) bars possess magnetic transparency and can be suitable for reinforcing structures that contain magnetic resonance imaging (MRI) equipment.

Many different types of FRP bars are commercially available, such as Glass FRP (GFRP), Carbon FRP (CFRP), and Aramid FRP (AFRP). The newly developed Basalt FRP (BFRP) bars are also drawing more attention due to their excellent mechanical behavior. However, wider application of the FRP bars in the construction industry is still limited. Unlike steel, FRP bars have low ductility and fail in a brittle manner. They exhibit a linear stress-strain relationship till failure. Furthermore, FRP bars are also characterized by low modulus of elasticity and relatively weak bond with concrete, which can yield large deflections and crack widths. Currently, procedures and guidelines for designing FRP reinforced structures are provided by codes like the ACI 440.1R [1] and CAN/CSA S806 [2].

With the increase in demand for FRP bars, there has been extensive research on the behavior of FRP reinforced concrete elements. The effect of different parameters, such as concrete strength and reinforcement ratio, has been investigated in the literature. However, a limited number of studies have examined the effect of using Ultra-High Strength Concrete (UHSC) with FRP bars. UHSC is an advanced composite material with superior strength and durability. Structures such as high-rise buildings and super-span bridges necessitates the need for this type of concrete. This is because it helps in providing safe, durable, and economical designs. The development of UHSC requires the use of high content of cementitious materials, low water-binder ratio, and steel fibers to achieve a very dense and homogenous microstructure with good ductility. UHSC can generally reach compressive strengths greater than 120 MPa. Although high strengths can result in brittle matrices, the incorporation of steel fibers ensures that the UHSC has adequate ductility.

Using UHSC in combination with FRP reinforcement can have several advantages. The use of FRP bars can solve the corrosion problem of steel reinforcement and improve the durability of concrete structures, while the use of UHSC can reduce the structural dimensions and the amount of reinforcement needed to carry the applied loads on the structure. Furthermore, the fibers in the UHSC matrix can enhance the ductility of members reinforced with FRP bars. Previous studies have also reported that the high tensile properties of the FRP bars were better utilized when higher concrete strengths were employed [3], [4]. In addition, the use of UHSC can improve the cracking response of FRP reinforced members.

1.3. Problem Statement

Fiber Reinforced Polymer (FRP) bars are one of the promising new developments in the construction field. They possess non-corrosive characteristics, which can help overcome the deficiencies of steel reinforcement and increase the service life of concrete structures. The FRP bars are also characterized with high strength to weight ratio and a linear stress-strain relationship. Thus, using concrete with high compressive strengths, such as UHSC, can result in maximum utilization of the high tensile strength of the FRP bars. The improved compressive strain of the UHSC allows the FRP bars to sustain larger strains and accordingly achieve higher strengths, which improves the ultimate capacity of flexural members. In addition, the presence

of fibers in the matrix of UHSC can enhance the ductility of FRP reinforced beams. However, there is still lack of studies on UHSC beams reinforced with FRP bars. Thus, this research aims to give an insight into the flexural behavior of this type of beams. Fifteen beams were prepared with UHSC and reinforced with GFRP, BFRP, and steel bars. The research investigated the serviceability behavior of UHSC-FRP beams including the midspan deflections and the cracking behavior, as well as the flexural response including the failure modes and ultimate capacities.

1.4. Thesis Objectives

The main objective of this study is to investigate the flexural behavior of beams constructed with UHSC and reinforced longitudinally with FRP bars. In general, normal strength concrete (NSC) beams reinforced with FRP bars fail at an ultimate compressive strain of 0.003. Using UHSC can allow the concrete strain to reach a value beyond 0.003, which leads to a greater exploitation of the tensile strength of the FRP bars, and improves the flexural capacity of the beams. Thus, the primary objectives of the research are listed below:

1) Investigate the serviceability and flexural behavior of UHSC beams reinforced with FRP bars in terms of failure modes, moment versus deflection behavior, cracking response, and strain values.
2) Investigate the effect of using different GFRP reinforcement ratios on the flexural response of UHSC beams.
3) Study the impact of using different numbers of GFRP reinforcing bars on the flexural behavior of UHSC beams, while maintaining the same reinforcement ratios.
4) Examine the effect of varying the surface texture of GFRP bars (ribbed and sand-coated) on the flexural response of UHSC beams.
5) Study the effect of using different reinforcement types on the behavior of UHSC beams in flexure.
6) Assess the applicability of the ACI 440.1R and CAN/CSA S806 recommendations for FRP-UHSC beams. Equations for finding cracking moment, flexural capacity, and midspan deflection are verified through comparison with experimental results.

1.5. Research Contribution

The use of FRP bars in concrete structures exposed to aggressive environments has been increasing due to their noncorrosive properties. They can solve the corrosion problem associated with steel reinforcement and result in more durable structures. Another benefit of the FRP bars is their high tensile strength. Previous studies showed that using concrete with high compressive strengths, like UHSC, can result in greater exploitation of the high tensile strength of FRP bars. The UHSC is also very ductile and can resist tensile and flexural loads due to the presence of fibers in this type of concrete. This, in turn, can enhance the poor ductility and large crack widths often encountered with FRP reinforced beams. There have been several studies on the flexural response of FRP reinforced beams developed with concrete strengths less than 100 MPa. However, the literature demonstrates that there are very limited studies investigating the flexural performance of beams with concrete strengths greater than 100 MPa. Also, there is a lack of studies on the flexural behavior of UHSC-BFRP beams as BFRP bars are relatively new and there is not much research on them. Thus, this research examined the use of GFRP bars and BFRP bars as longitudinal reinforcement in UHSC beams subjected to flexural loads. Effect of reinforcement type, ratio, surface texture, and number of bars was studied. Experimental results were used to validate the accuracy of the ACI 440.1R and CAN/CSA codes and their applicability for beams with concrete strengths exceeding 100 MPa.

1.6. Thesis Organization

The rest of the thesis is organized as follows: Chapter 2 provides background information on the properties of both FRP and UHSC composite materials. It also summarizes the recent studies on the flexural behavior of FRP reinforced beams. Chapter 3 presents the proposed experimental program including the design considerations and equations, the beam detailing, the test matrix, the material properties, and the testing setup. Chapter 4 analyses and discusses the results and chapter 5 concludes the thesis.

Chapter 2. Background and Literature Review

This chapter discusses the mechanical and physical properties of FRP bars. The chapter also discusses the properties of the UHSC composite material. Then, an extensive review of the existing research on HSC and UHSC beams reinforced with FRP bars is presented, and gaps in knowledge are identified.

2.1. Physical and Mechanical Properties of FRP Bars

Over the decades, the demand on the FRP material has increased due to their excellent corrosion resistance, high tensile strength, and light weight. FRP material is a composite material that is produced from small-diameter fibers bound together using either epoxy or vinyl ester to produce a synergistic material [5]. The FRP bars are made of different types of fibers such as glass, aramid, carbon, or basalt fibers. The most commonly used FRP bars are the GFRP bars due to their cheap cost. They are also non-conductive to electricity and non-magnetic in nature. On the other hand, BFRP bars are one of the recent developments in the composite material market. There is still ongoing research on the BFRP reinforcement as they are relatively new. Both the GFRP and BFRP bars have very similar chemical compositions. However, the basalt has a large amount of iron giving it a very dark color [6]. Moreover, the BFRP material has various advantages as compared to other reinforcement types. For example, the BFRP bars have much higher tensile strength than steel bars with only one-third of their density [6]. The production of the basalt fibers is more eco-friendly and cheaper than that of carbon fibers. In addition, basalt fibers have higher energy absorption capacities as compared to glass and carbon fibers [7]. The properties of the BFRP and GFRP bars were examined in several studies including their tensile and compressive characteristics [8], [9], as well as their bond properties [10], [11]. There are various factors that play an important role in defining the properties of the FRP material including the fiber volume fraction, type of resin and its properties, and the fiber orientation. Thus, there are no universal mechanical property values for FRP reinforcing bars as it differs from one manufacturer to another [12].

The physical and mechanical characteristics of steel and FRP bars are different. While steel reinforcement is isotropic in nature, the FRP bars are anisotropic and possess high tensile strength only in the direction of the fibers. This impacts the shear

capacity, dowel action, and bond performance of the FRP bars. In addition, the FRP reinforcement have a linear behavior up to failure with no definite yielding point, which results in a brittle failure (Refer to Figure 2-1). The modulus of elasticity of the FRP bars is also much lower than that of steel bars and they have lower creep-rupture threshold. Since the properties of the FRP bars differ from that of steel, changes in the traditional design philosophy of reinforced concrete (RC) structures are required. Hence, a number of standards and design guides have been published by the United States, Canada, Europe, and Japan for FRP reinforced concrete structures [1].

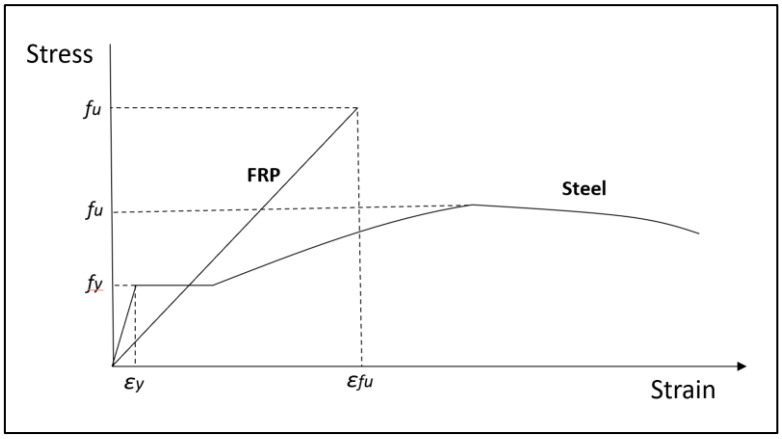

Figure 2-1: Stress-strain curves of FRP and steel bars.

2.2. Ultra-High Strength Concrete (UHSC)

The recent advancements in the material technology led to the development of different types of concrete, one of which is the Ultra High Strength Concrete (UHSC). UHSC is an advanced composite material with superior properties. It is produced by mixing powders (Portland cement, silica fume, and quartz flour), as well as high-range water reducers, and fibers [13]. The mixing of fine materials results in a very dense matrix, which allows the UHSC to achieve its exceptional strength, stiffness, and durability. Hence, the high compressive strength of the UHSC can be attributed to two main factors: fine packing of the material particles and low water to binder ratio. The UHSC has compressive strengths ranging between 120 and 150 MPa, and flexural strengths ranging between 15 to 25 MPa. Its modulus of elasticity ranges between 45 and 50 GPa [13].

Although high strengths can result in brittle matrices, the incorporation of fibers ensures that the UHSC has adequate ductility and can achieve high flexural strengths.

Fiber types generally used in the UHSC include steel, PVA, glass, or carbon. Thus, the UHSC can support tensile and flexural loads, even after cracking occurs. Furthermore, the highly compacted and dense matrix of this concrete results in low permeability to harmful materials like chlorides [13]. This enhances the durability characteristics of the UHSC and makes it suitable for harsh and aggressive environments. The UHSC can be used for building new structures or for strengthening and rehabilitating existing structures.

Despite the superior mechanical properties of UHSC, there are several concerns about its application. For instance, the low water to binder ratio and high cementitious contents, can lead to large autogenous shrinkage. Also, one of the major reasons limiting the use of UHSC is that its manufacturing process has high carbon footprint due to the large quantities of cement needed for its development. In addition, the initial cost of UHSC is higher than conventional concrete, but the overall costs might be lower as it can help in reducing the sizes and dimensions of concrete elements and the amount of reinforcement required.

2.3. Literature Review

2.3.1 Normal strength concrete (NSC) with FRP bars

Extensive studies have been conducted on concrete members cast with NSC and reinforced with FRP bars. Some studies investigated the contribution of FRP bars to the ultimate capacity of RC columns [14], [15]. Elmesalami et al. [14] found that the FRP bars contributed around 11% to the load carrying capacity of concentrically loaded columns and that ignoring the strength contribution of FRP bars led to conservative predictions. In another study, Alnajmi and Abed [15] found that the contribution of FRP bars to the ultimate capacities of RC columns depended on the amount of reinforcement, and reached up to 24% for high reinforcement ratios.

The shear performance of FRP reinforced beams was also examined [16]–[18]. El Refai and Abed [16] studied the shear response of beams with BFRP bars and found that BFRP reinforced beams had similar behavior to GFRP and AFRP reinforced beams. They also reported that the contribution of concrete to the shear strength of FRP reinforced beams decreased with an increasing shear span to depth ratio. Abed et al. [17] examined the shear behavior of FRP reinforced beams with basalt microfibers

incorporated into the concrete mix. It was concluded that the load carrying capacity of the beams improved by 42% upon the addition of the basalt fibers.

There have also been several studies on the flexural behavior of FRP reinforced beams [19]–[24]. El-Nemr et al. [19] examined the flexural and serviceability behavior of RC beams with GFRP bars. A total of 17 beams were prepared and tested under four-point loading. The beams had 4,250 mm length, 200 mm width, and 400 mm depth. The experimental results revealed that the sand-coated GFRP bars had better cracking behavior than helically-grooved bars due to their uniform surface texture. In addition, increasing the axial stiffness enhanced the flexural capacity of the beams, and reduced the midspan deflections and crack widths. The authors also found that using smaller bar diameter, while maintaining the same axial stiffness, improved the strain and cracking response of the tested specimens due to smaller bar spacing. In another study, Chellapandian et al. [20] examined the use of different volumes of macro-synthetic fibers on the flexural behavior of GFRP reinforced beams. It was found that the addition of 1% of fibers improved the deformability of the tested beams and changed the failure mode from brittle flexure-shear to ductile flexure failure.

Elgabbas et al. [21] studied the flexural performance of concrete beams reinforced with BFRP bars. The authors varied the reinforcement ratio by using three different diameters of the BFRP bars: 10, 12 and 16 mm. It was found that beams with low reinforcement ratios displayed large increases in strains and midspan deflections once cracking occurred. As the axial stiffness increased, the beams reported lower deflections, strains, and narrower cracks at the same loading level.

Abed and Alhafiz [22] examined the effect of adding different kinds of fibers on the flexural response of concrete beams with BFRP bars. The authors used plain concrete, as well as basalt, and synthetic fiber reinforced concrete. The experimental results showed that the addition of fibers led to a significant increase in the moment capacities. This is because the fibers improved the concrete compressive strain, which allowed the BFRP bars to achieve higher tensile strengths. The bridging effect of the fibers also helped in limiting the propagation of the cracks. The authors also found that increasing the number of tensile bars, while maintaining same reinforcement ratio, improved the cracking behavior and curvature ductility of the FRP reinforced

beams, but it did not affect their moment capacity. Furthermore, the FRP reinforced beams had deeper and larger number of cracks than their steel counterparts.

El Refai et al. [23] studied the flexural performance of concrete beams reinforced with hybrid bars (GFRP and steel). The study consisted of nine beams in total, each measuring 230 X 300 mm in cross-sectional area and 4000 mm in length. The results revealed that hybrid reinforced concrete beams had better deformability, cracking response, and flexural capacity than the beams with GFRP reinforcement only.

2.3.2 High strength concrete (HSC) with FRP bars

Many studies have been carried out on the flexural response of HSC beams reinforced with FRP bars [3], [4], [25]–[35]. For example, Adam et al. [25] studied the flexural performance of ten GFRP reinforced beams with varying concrete strengths. The beams were tested in a four-point loading setup. Experimental results showed that increasing the concrete strength from 25 to 70 MPa reduced the crack widths by around 80%. Furthermore, the increase in concrete strength improved the flexural capacity of the over-reinforced beams, where it jumped from 75.2 kN to 145.1 kN. The authors also found that the ACI 440.1R-06 and CSA S806 codes underestimated the midspan deflections, especially for beams with low GFRP ratios, but the CSA S806 was more conservative.

Similarly, Theriault and Benmokrane [26] tested 12 concrete beams under four-point flexural loading. The concrete strengths ranged between 46.2 and 97.4 MPa. Two different reinforcement ratios, 1.16% and 2.77%, were used for each concrete strength. The authors concluded that using higher concrete strengths and reinforcement ratios can increase the ultimate capacity of the FRP reinforced beams, but the increase is limited by the concrete strain.

Abdelkarim et al. [27] aimed to investigate the behavior of NSC and HSC beams reinforced with GFRP bars. The experimental program consisted of eight beams in total, four of them were developed with 35 MPa concrete, and the other four with 65 MPa concrete. The test results showed that increasing the concrete strength yielded a 41.2% increase in the moment capacity. The cracking response of the specimens was also enhanced upon increasing the concrete strength. However, the HSC beams reported larger maximum deflections as compared to their NSC counterparts.

In another study, El-Nemr et al. [4] conducted a thorough investigation on the flexural performance of GFRP reinforced beams. The main parameters in the study were the GFRP reinforcement ratio, the bar sizes, the compressive strength of concrete, and the surface configuration of the GFRP bars. In the study, concrete strengths of 30 and 65 MPa were utilized for the NSC and HSC beams, respectively. After applying four-point loading to the beams, several conclusions were drawn. First, it was found that both the NSC and HSC beams behaved in a similar manner up to failure, but the HSC beams showed enhanced post-cracking stiffnesses. In addition, the HSC beams had higher cracking moments than the NSC beams, which was expected as the cracking moment is directly related to the compressive strength of concrete. For the HSC beams, the ultimate capacity increased by 116%, with the increase in the reinforcement ratio from 0.55 to 1.78%. This significant increase was due to the change in failure mode from FRP bar rupturing to concrete crushing. However, the authors recommended that a minimum reinforcement ratio must be kept in order to satisfy the serviceability limits, even if the beams were over-reinforced.

Yang et al. [28] reported better ductility, higher flexural strength, and reduced crack widths for HSC beams reinforced with FRP bars, when fibers were added to the concrete mix. The beams with fibers also exhibited significant inelastic deformations, near failure, due to the softened post peak behavior of this type of concrete. However, the authors noted that the increased compressive strain of the fiber reinforced concrete (FRC) caused some of the beams to fail by FRP rupture, despite the beams being designed to be compression-controlled.

A study was conducted by Esfahani and Sharbatdar [29] on ten beams reinforced with GFRP bars. The main purpose of the study was to examine the effect of replacing conventional concrete with high-performance fiber-reinforced cementitious composite (HPFRCC). The HPFRCC had an average compressive strength of 59 MPa. It was found that the use of HPFRCC changed the mode of failure from brittle to ductile and increased the energy absorption capacity up to 120% for the GFRP reinforced beams.

Rashid et al. [30] performed flexural tests on a series of HSC beams reinforced with AFRP bars. The beams had 150 mm X 300 mm cross-sections and were 3000 mm in length. The most important parameters considered were the concrete strength, reinforcement ratio, as well as the type and extent of confinement provided to the

compression zone of the section. Two types of confinements were utilized in the experimental program, lateral ties and PVA fibers. After performing three-point loading tests, the experimental results showed that AFRP reinforced beams had significantly larger crack widths and deflections compared to their steel counterparts. The results also showed that the ductility of the AFRP reinforced beams was enhanced by either increasing the amount of tensile reinforcement or adding more confinement to the compression zone through lateral ties.

A study conducted by Abed et al. [3] examined the flexural properties of HSC beams reinforced with FRP bars. For comparison purposes, BFRP bars with different diameters (8, 10, 12, and 16 mm) and CFRP bars with 12 mm diameter were utilized as tensile reinforcement in the concrete beams. The NSC and HSC had compressive strengths of 47.5 and 70.5 MPa, respectively. The authors found out that increasing the strength of concrete enhanced the cracking and ultimate moments by around 10 and 16%, respectively. Furthermore, replacing steel with FRP bars in HSC beams increased the flexural capacities by 130%, which indicates that the use of HSC was more beneficial in FRP reinforced beams than in steel reinforced beams. It was also concluded that for the same axial stiffness, the use of smaller bar diameters yielded in lower midspan deflections.

Zhu et al. [31] investigated the flexural response of partially fiber-reinforced beams that were developed with HSC and reinforced with FRP bars. The experimental results revealed that the addition of fibers to the tensile zone reduced the deflection and crack width of the tested beams. However, the incorporation of fibers to only the tensile zone led to a reduced ductility of the FRP reinforced beams. Therefore, the authors recommended that steel fibers are to be added to the full depth of structures, in particular for RC structures where high ductility is required. Moreover, beams that were fully reinforced with steel fibers had significantly larger section capacity than beams that were only partially reinforced.

A study conducted by Moawad and Fawzi [32] aimed to investigate the performance of six concrete beams reinforced with GFRP bars in flexure. Each specimen had 150 mm X 200 mm cross-sectional area and 1700 mm clear span length. Two concrete compressive strengths were employed in the study: 30 MPa and 60 MPa. The test results showed that replacing steel reinforcement with GFRP bars increased the load

carrying capacity of the beams and reduced the number of cracks. However, the steel reinforced beams reported higher ductility and smaller crack widths than the FRP reinforced beams. In addition, increasing the concrete compressive strength decreased the ductility by 15.14% for the GFRP reinforced beams.

Yinghao and Yong [33] studied the effect of using hybrid reinforcement (GFRP and steel bars) on the flexural behavior of HSC beams. The authors found that the maximum crack width depended mainly on the depth of the steel reinforcement. By increasing the depth of the steel bars, the maximum crack width was reduced. However, increasing the depth of the steel layer led to an increase in the deflection of hybrid reinforced beams, given a particular load level.

Therefore, the review of literature shows that using HSC in place of NSC can make a greater use of the high tensile strength of FRP bars, and improve the ultimate capacity of the beams. The previous studies also show that the cracking response and ductility of FRP reinforced beams can be enhanced by using HSC with fibers.

2.3.3 Ultra-high strength concrete (UHSC) with FRP bars

In recent years, few studies have focused on examining the influence of using UHSC with FRP bars [36]–[39]. For example, Goldston et al. [36] developed HSC and UHSC beams reinforced with GFRP bars. The flexural behavior was measured in terms of ultimate capacity, deflection, energy absorption, and failure modes. A total of six beams reinforced with GFRP bars were tested under three-point bending. The authors found that increasing the strength of concrete from 95 MPa to 117 MPa, increased the ultimate capacity for over-reinforced beams, but had negligible effect on under-reinforced beams. This is because GFRP rupture is the governing mode of failure in under-reinforced beams. In addition, some amount of pseudo ductility was observed in over-reinforced beams, where the beams carried additional load after the concrete crushed. The authors deduced that the ACI and CSA codes resulted in very conservative predictions for the load-carrying capacity of the beams. However, the two codes were unconservative when predicting the midspan deflection of the beams at the ultimate load level. Hence, there is a need for further improvement of the guidelines for the design of UHSC beams with FRP reinforcement.

Yoo et al. [37] investigated the service deflection of GFRP reinforced beams made with ultra-high performance fiber reinforced concrete (UHPFRC). The concrete had a strength of 197.3 MPa, and the reinforcement ratio of the beams ranged between 0.53 and 1.71%. The authors found that the UHPFRC beams maintained stiff load-deflection curves post cracking, which proves that UHPFRC can effectively reduce the deflection of FRP reinforced beams. In addition, only very fine microcracks formed up to near the ultimate load. This can be attributed to the steel fibers present in the UHPFRC, which can resist some of the tensile stress applied on the beam. Increasing the reinforcement ratio reduced the crack widths at a specific load level, but the crack spacing and number of cracks were not affected by the reinforcement ratio. Also, higher reinforcement ratios improved the flexural behavior of the beams in terms of higher bending stiffness, ultimate capacity, and ductility.

In another study, Yoo et al. [38] studied the flexural performance of UHPFRC beams reinforced with GFRP bars or hybrid reinforcement (steel and GFRP bars). It was found that all the tested specimens had very stiff load-deflection responses after cracking and satisfied the serviceability limit states. However, the authors concluded that the use of hybrid reinforcement did not lead to a remarkable improvement in the flexural behavior of UHPFRC beams. Hence, the authors recommended using only GFRP reinforcing bars with UHPFRC rather than using both steel and GFRP reinforcement.

The previous studies show that using UHSC in FRP reinforced beams can have a positive influence on their ultimate capacity, ductility, and serviceability. However, the studies conducted on UHSC beams reinforced with FRP bars are very limited. Also, there is a significant need to improve the guidelines and specifications related to this type of beams. Therefore, this study aims to investigate the flexural behavior of beams developed with UHSC and reinforced longitudinally with FRP bars. Experimental results were used to assess the accuracy of the ACI 440 and CAN/CSA S806 equations and provide recommendations.

Chapter 3. Experimental Program

This chapter presents the experimental program followed in this study including the design considerations and equations, beam detailing, material properties, and testing setup.

3.1. Design Considerations

In this section, the main factors considered when designing steel and FRP reinforced beams are stated. The design of steel and FRP reinforced beams was in accordance with the ACI 318 [40] and ACI 440.1R [1] codes, respectively.

3.1.1 Design of steel reinforced concrete beams

The design of the steel-reinforced beams was per the ACI 318 code [40]. These beams can either fail by concrete crushing or by steel yielding. When a section is tension controlled, the beams experience tensile yielding, whereas when the section is compression controlled, concrete crushing occurs. Tension-controlled sections are sections with reinforcement ratios lower than the balanced ratio. On the other hand, compression-controlled sections are sections where the reinforcement ratio is greater than the balanced ratio. According to ACI 318, only tension-controlled sections are permitted in the design as they display some warning before failure. Beams in the balanced zone fail by concrete crushing and steel yielding simultaneously. Figure 3-1 illustrates the reduction factors for the different types of sections.

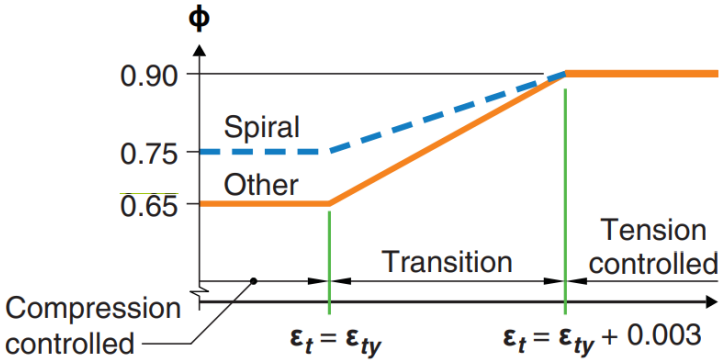

Figure 3-1: Strength reduction factor for steel reinforced beams [40].

Since compression-controlled sections have a catastrophic failure, they have a reduction factor of 0.65, while the tension-controlled sections have a reduction factor of 0.9. The reduction factor helps to account for various issues, such as uncertainties

in the material properties. Steel reinforced beams in this study were under-reinforced or tension-controlled to achieve ductile behavior as recommended by the ACI 318 code.

3.1.2 Design of FRP reinforced concrete beams

The ACI 440.1R [1] allows the design of FRP reinforced beams as under-reinforced or over-reinforced. However, the practice of designing FRP reinforced concrete beams to be over-reinforced is encouraged as it provides a degree of deformability prior to failure. These beams can experience two failure modes: concrete crushing and FRP rupture. Concrete crushing occurs when the reinforcement ratio is greater than the balanced ratio ($\rho_f > \rho_{fb}$), whereas FRP rupture occurs when the FRP ratio is less than the balanced ratio ($\rho_f < \rho_{fb}$). If a beam has a reinforcement ratio equal to the balanced ratio, it will fail by concrete crushing and FRP rupture simultaneously. However, the code defined a compression-controlled section as one where $\rho_f \geq 1.4\,\rho_{fb}$, and a tension-controlled section is defined as a section in which $\rho_f \leq \rho_{fb}$. The code states that a flexural member with $\rho_{fb} < \rho_f < 1.4\,\rho_{fb}$ will theoretically be controlled by concrete crushing, but a lower reduction factor should be used compared to that of a compression-controlled section. This is because there is a possibility that such sections might fail due to FRP rupture, if the actual strength of concrete is higher than specified or due to other reasons. The strength reduction factors are demonstrated in Figure 3-2.

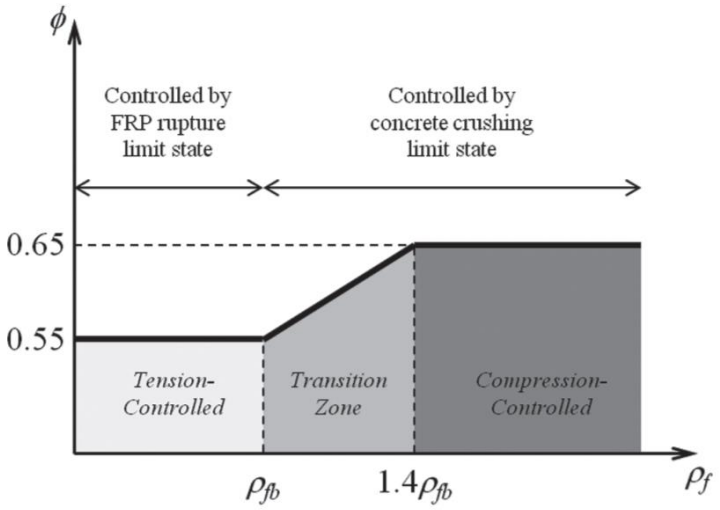

Figure 3-2: Strength reduction factors for FRP reinforced beams [1].

FRP reinforced specimens have smaller reduction factors than their steel counterparts as they exhibit less ductility. The following section explains the equations used in the design of those beams, which depends on whether they are under-reinforced or over-reinforced. In this research, both under-reinforced and over-reinforced beams were cast and tested to examine the differences in their responses.

3.2. Design Code Equations of Steel RC Beams

The steel reinforced concrete beams are designed as tension controlled using the ACI 318 code [40]. Equation 1 shows how the flexural capacity is calculated:

$$M_n = A_s f_y (d - \frac{a}{2}) \quad (1)$$

where:

A_s is the total area of steel reinforcement used in the section (mm^2).

f_y is the yield strength of steel (MPa).

d is the effective depth of the beam (mm).

a is the depth of the equivalent rectangular concrete stress block (mm), and can be computed using Equation 2:

$$a = \frac{A_s f_y}{0.85 f'c\, b} \quad (2)$$

where:

$f'c$ is the concrete compressive strength (MPa).

b is the width of the beam (mm).

A strength reduction factor of 0.9 is used to adjust the moment capacity of the beams. The reduction factor considers uncertainties arising from the materials used, inaccurate design calculations, and other factors.

3.3. Design Code Equations of FRP RC Beams

The ACI440.1R code states that the FRP reinforced beams can fail by either concrete crushing or FRP rupture. Beams with a reinforcement ratio lower than the balanced reinforcement ratio experience failure due to FRP rupture. Such type of failure is not recommended as it is abrupt. On the other hand, the compressive failure due to

concrete crushing gives more warning prior to failure. In this study, the FRP reinforced beams were designed as tension-controlled and compression-controlled to study both types of failure modes. The balanced reinforcement ratio can be calculated using Equation 3:

$$\rho_{fb} = 0.85\,\beta_1 \frac{f'c}{f_{fu}} \left(\frac{E_f\,\varepsilon_{cu}}{E_f\,\varepsilon_{cu} + f_{fu}}\right) \tag{3}$$

where:

f_{fu} is the design tensile strength of the FRP reinforcement (MPa).

E_f is the elastic modulus of the FRP reinforcement (MPa).

ε_{cu} is the ultimate compressive strain of concrete.

β_1 is the ratio of the depth of the Whitney block to the depth of the neutral axis and can be found using Equation 4.

$$\beta_1 = \begin{cases} 0.85 & for\ (f'c \leq 28\ MPa) \\ 0.85 - 0.05\left(\dfrac{f'c - 28}{7}\right) & for\ (28\ MPa < f'c < 56\ MPa) \\ 0.65 & for\ (f'c\ \geq 56\ MPa) \end{cases} \tag{4}$$

The reinforcement ratio of the beam section can be found using Equation 5:

$$\rho_f = \frac{A_f}{b\,d} \tag{5}$$

where A_f is the total area of the FRP reinforcement (mm^2).

The flexural capacity of the beams is computed based on the assumptions listed below:

1. A plane section before loading remains plane after loading. This indicates that the concrete and FRP strains are directly proportional to the distance from the neutral axis.
2. The concrete tensile strength is neglected.
3. The value of the maximum usable compressive strain of concrete is 0.003.
4. FRP bars have a linear elastic behavior up to failure with no clear yielding point.
5. There is a perfect bond between the concrete and the FRP bars.

3.3.1 Flexural capacity

For over-reinforced beams, where concrete crushing is the governing failure mode, the stress-strain distribution of the concrete can be represented by the Whitney block shown in Figure 3-3.

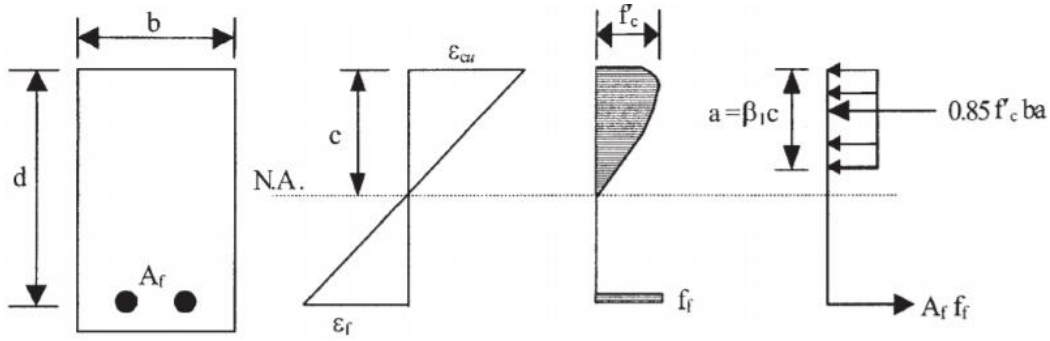

Figure 3-3: Failure by concrete crushing [1].

The nominal flexural strength of the beam section can be found in terms of the FRP reinforcement ratio through Equation 6:

$$M_n = \rho_f f_f \left(1 - 0.59 \frac{\rho_f f_f}{f'c}\right) b d^2 \tag{6}$$

where f_f is the stress in the FRP reinforcement and can be found using Equation 7.

$$f_f = \left(\sqrt{\frac{(E_f \varepsilon_{cu})^2}{4} + \frac{0.85 \beta_1 f'c}{\rho_f} E_f \varepsilon_{cu}} - 0.5 E_f \varepsilon_{cu}\right) \leq f_{fu} \tag{7}$$

When the FRP reinforcement ratio is less than the balanced ratio, the beam sections are under-reinforced, and they fail by FRP rupture. The stress-strain distribution for the under-reinforced concrete sections can be seen in Figure 3-4.

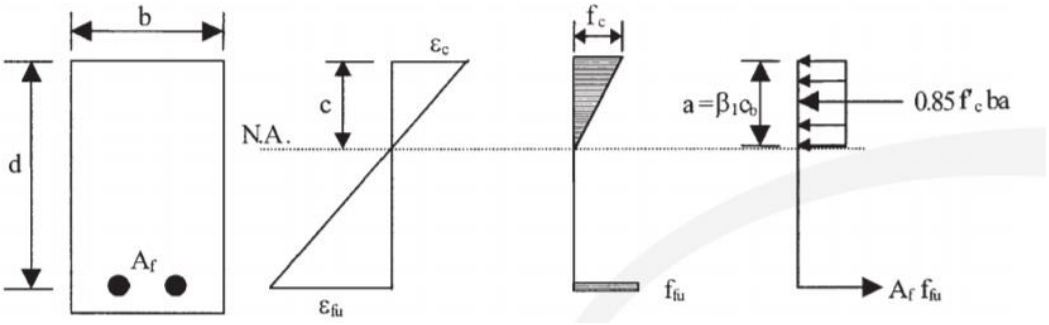

Figure 3-4: Failure by FRP rupture [1].

Equation 8 can be used to compute the nominal flexural capacity of the section.

$$M_n = A_f f_{fu} (d - \frac{\beta_1 c_b}{2}) \quad (8)$$

where c_b is the distance from the extreme compression fiber to the neutral axis at balanced strain conditions (mm). It can be found using Equation 9:

$$c_b = \left(\frac{\varepsilon_{cu}}{\varepsilon_{cu} + \varepsilon_{fu}}\right) d \quad (9)$$

For all beam sections, under-reinforced and over-reinforced, the applied moment must be less than or equal to the nominal flexural capacity of the beams ($M_u \leq \phi M_n$). Like steel reinforced beams, a strength reduction factor is applied to the nominal capacity to account for any uncertainties in the materials used and the brittle behavior of FRP members. The ACI 440.1R code imposes a strength reduction factor of 0.65 for compression-controlled sections ($\rho_f \geq 1.4 \rho_{fb}$), and 0.55 for tension-controlled sections ($\rho_f \leq \rho_{fb}$). The reduction factor for sections that are in the transition zone ($\rho_{fb} < \rho_f < 1.4 \rho_{fb}$) can be represented using Equation 10:

$$0.3 + 0.25 \frac{\rho_f}{\rho_{fb}} \quad (10)$$

3.3.2 Cracking moment

Cracking moment is defined as the moment at which cracking of the concrete would start. The cracking moment can be found using Equation 11:

$$M_{cr} = \frac{2 f_r I_g}{h} \quad (11)$$

where:

M_{cr} is the first cracking bending moment (N.mm).

h is the depth of the beam (mm).

I_g is the gross moment of inertia (mm^4), calculated using Equation 12:

$$I_g = \frac{b h^3}{12} \quad (12)$$

f_r is the modulus of rupture of concrete (MPa). It can be found using Equation 13 for the ACI 440.1R-15 and Equation 14 for the CAN/CSA S806-12:

$$f_r = 0.62 \lambda \sqrt{f'c} \quad (13)$$

$$f_r = 0.60\,\lambda\sqrt{f'c} \tag{14}$$

where λ is a modification factor for lightweight concrete. It has a value of 1 for normal weight concrete.

3.3.3 Deflection

According to the ACI 440.1R code, the deflection of FRP reinforced beams under four-point loading can be determined using Equations 15-19:

$$\Delta_i = \frac{P\,a}{48\,E_c\,I_e}\,(3L^2 - 4a^2) \tag{15}$$

$$I_e = \frac{I_{cr}}{1 - \gamma\left(\frac{M_{cr}}{M_a}\right)^2\left[1 - \frac{I_{cr}}{I_g}\right]} \tag{16}$$

$$\gamma = 1.72 - 0.72\,(\frac{M_{cr}}{M_a}) \tag{17}$$

$$I_{cr} = \frac{b\,d^3}{3}\,k^3 + n_f\,A_f\,d^2\,(1-k)^2 \tag{18}$$

$$k = \sqrt{2\,\rho_f\,n_f + \left(\rho_f\,n_f\right)^2} - \rho_f\,n_f \tag{19}$$

where:

Δ_i is the midspan deflection (mm).

P is the applied concentrated load (N).

a is the beam shear span (mm).

E_c is the elastic modulus of concrete (MPa).

I_e is the effective moment of inertia (mm^4).

M_a is the applied maximum moment (N.mm).

I_{cr} is the moment of inertia of transformed cracked section (mm^4).

L is the length of span (mm).

n_f is the ratio of modulus of elasticity of FRP reinforcement to the modulus of elasticity of concrete.

k is the ratio of depth of neutral axis to reinforcement depth.

The midspan deflection can be determined using the CAN/CSA S806 code by applying Equations 20-22:

$$\Delta_i = \frac{P\,L^3}{48\,E_c\,I_{cr}}\left[3\left(\frac{a}{L}\right) - 4\left(\frac{a}{L}\right)^3 - 8\,\eta\left(\frac{L_g}{L}\right)^3\right] \tag{20}$$

$$\eta = 1 - \left(\frac{I_{cr}}{I_g}\right) \tag{21}$$

where L_g is the uncracked length in half of the beam and can be found using Equation 22:

$$L_g = a\left(\frac{M_{cr}}{M_a}\right) \tag{22}$$

3.4. Beam Detailing

To achieve the research objectives, a total of 15 beams were cast and tested under flexural loading. Each beam had a rectangular cross-section of 185 mm in width by 250 mm in depth, as shown in Figure 3-5. All the ACI 440.1R-15 code recommendations related to the number of bars, size of the bars, bar spacing, and clear cover were considered during the design of the beam's cross-section. The design also considers the minimum required depth (one-tenth of the effective span) and ensures slender specimens, where the shear span to effective depth ratio (a/d) has a value greater than 3. A clear cover of 30 mm from the bottom was chosen to provide sufficient protection against any external exposure conditions. The clear cover was 25 mm from the top compression fibers and 27.5 mm from each side. Two or three longitudinal bars were used in the tensile zone of each beam specimen.

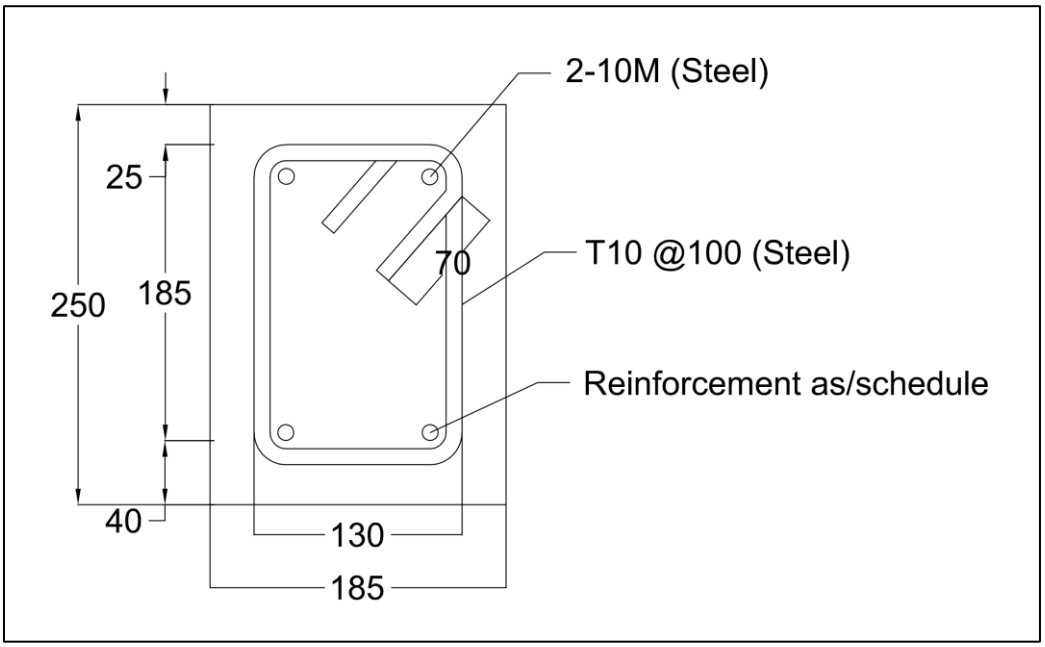

Figure 3-5: Beam's cross section.

The beam's dimensions and design should guarantee that it will fail purely in flexure and prevent any unwarranted modes of failure. To avoid shear failure, 10 mm steel stirrups were provided throughout the beam's shear span and spaced evenly at 100 mm centers. Two steel bars were placed in the compressive zone of each beam to act as hungers for the stirrups. As depicted in Figure 3-6, the beams had a pure moment region of 400 mm without any stirrups and a clear span of 1900 mm. An additional extension of 150 mm was provided on each side of the beam, which resulted in a total span of 2200 mm, to ensure sufficient development length for the FRP bars.

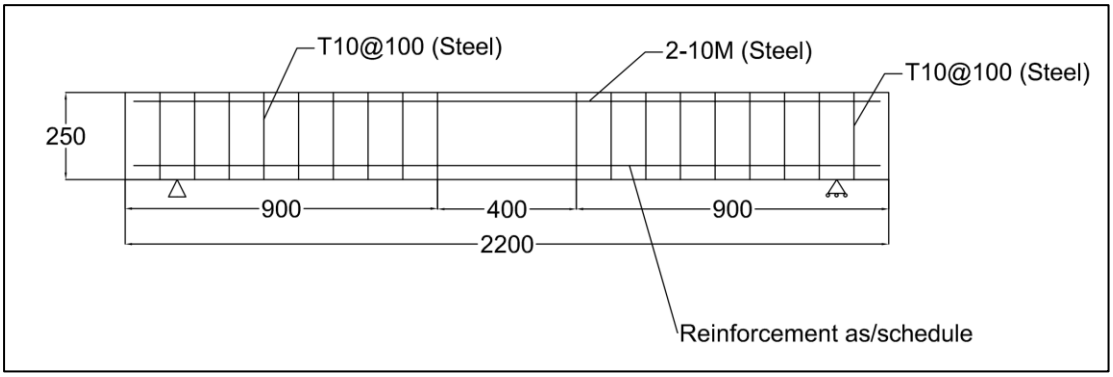

Figure 3-6: Beam's elevation.

3.5. Test Matrix

In this study, fifteen beams were cast and experimentally tested under four-point loading. The details of each beam are listed in Table 3-1. The beams were prepared using concrete with a target compressive strength of 140 MPa. Beams with ρ_f/ρ_{fb} ratio less than 1 were tension-controlled or under-reinforced, whereas beams with ρ_f/ρ_{fb} ratio greater than 1 were compression-controlled or over-reinforced. Although beam 3T10G was designed as under-reinforced, the actual FRP bar diameter in this beam, 10.95 mm, resulted in the ρ_f/ρ_{fb} ratio being very close to 1, which represents a section in the balanced zone.

Each UHSC beam was identified using a set of numbers and letters, where the first number represents the number of longitudinal bars in the tensile zone, the second number represents the bar diameter in millimeters, and the last letter signifies the type of reinforcement (G – sand-coated GFRP, GR – ribbed GFRP, B – BFRP, S – steel). For example, 2T8G corresponds to a beam reinforced with two sand-coated GFRP

bars that are 8 mm in diameter. Some of the beams were duplicated to improve the accuracy of the results and are denoted by the letter 'D' at the end.

Table 3-1: Test matrix details.

Beam	Bar Type	Bar size (mm)	Area (mm^2)	EA (MN)	ρ_f(%)	ρ_f/ρ_{fb}
2T8G	GFRP	7.98	100.13	4.50	0.0026	0.36
2T8G-D	GFRP	7.98	100.13	4.50	0.0026	0.36
2T10G	GFRP	10.95	188.22	8.45	0.0050	0.65
2T12G	GFRP	12.42	242.40	10.88	0.0064	0.87
2T16G	GFRP	16.02	403.33	18.11	0.0108	1.16
2T20G	GFRP	20.35	650.67	29.21	0.0176	1.53
3T8G	GFRP	7.98	150.20	6.74	0.0039	0.54
3T10G	GFRP	10.95	282.33	12.68	0.0075	0.98
3T10G-D	GFRP	10.95	282.33	12.68	0.0075	0.98
2T12GR	GFRP	11.23	198.00	8.89	0.0052	0.51
2T10B	BFRP	10.09	160.09	6.85	0.0042	0.66
2T20B	BFRP	20.44	656.06	30.11	0.0178	2.07
2T12S	Steel	11.85	220.53	44.11	0.0058	0.11
2T12S-D	Steel	11.85	220.53	44.11	0.0058	0.11
2T16S	Steel	15.79	391.61	78.32	0.0105	0.19

The major variables considered in this study were the reinforcement ratio, the surface texture, the number of bars, and the reinforcement type. The effect of the reinforcement ratio was examined by comparing the GFRP reinforced beams (2T8G, 2T10G, 2T12G, 2T16G, and 2T20G) among each other. The reinforcement ratios ranged between 0.0026% and 0.0176%. Three of the beam specimens (2T8G, 2T10G, and 2T12G) were under-reinforced with $\rho_f \ / \ \rho_{fb}$ ratios below 1. Thus, these beams were expected to fail by FRP rupture. On the other hand, the 2T16G and 2T20G beams were over-reinforced with $\rho_f \ / \ \rho_{fb}$ ratios greater than 1, and were expected to fail by concrete crushing.

The effect of the GFRP surface texture was studied by analysing the beams reinforced with No. 12 ribbed and sand-coated GFRP bars (2T12GR and 2T12G). The effect of the number of bars was studied by analysing beams with the same reinforcement ratio, but different number of longitudinal bars in the tensile zone. Thus, the 2T10G beam was compared against the 3T8G beam, and the 2T12G beam was compared against the 3T10G beam.

The effect of the reinforcement type was studied by comparing beams with different types of tensile reinforcement. The beams reinforced with sand-coated GFRP bars (2T10G and 2T20G) were compared against those reinforced with BFRP bars (2T10B and 2T20B). In addition, steel reinforced beams were cast and tested to compare the behavior of UHSC beams reinforced with GFRP bars (2T12G and 2T16G) to those reinforced with steel bars (2T12S and 2T16S). The major variables in the study and the set of beams considered for each variable are presented in Figure 3-7.

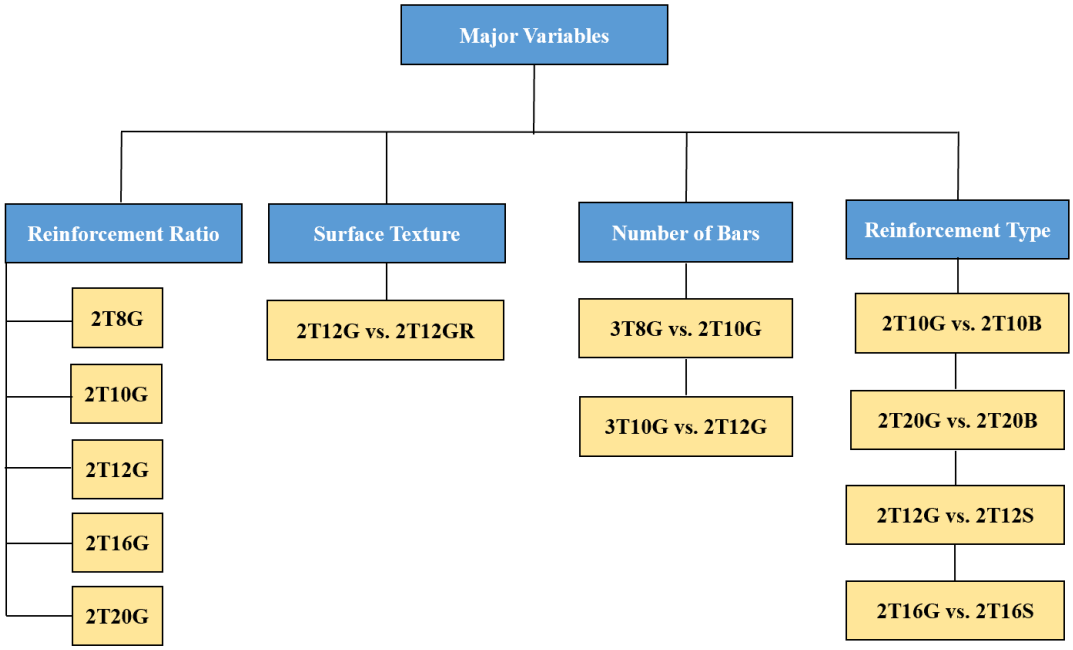

Figure 3-7: Major variables considered in this study.

3.6. Material Properties

In this section, properties of the materials used in the study are presented. These properties were either obtained from experimental testing or from the manufacturer specifications. The materials included in the experimental program are concrete, steel, BFRP, and GFRP reinforcement.

3.6.1 Concrete

The beams were cast using ready mixed concrete with a target compressive strength of 140 MPa. Steel fibers were added to the concrete mix. Table 3-2 displays the concrete mix design for the specimens as provided by Transgulf Readymix Concrete. Glenium 110 UNR was used as a superplasticizer to produce flowable concrete with significantly reduced water demand.

Table 3-2: Concrete mix design.

Unit Weight (kg/m3)							
Cement	Water	20 mm Agg.	10 mm Agg.	Washed Sand	Dune Sand	M. Silica	Superplasticizer
700	140	560	365	450	305	150	10

On the day of testing, the actual concrete strength was determined by testing three concrete cylinders, each with 150 mm diameter and 300 mm height. Three cubes of 150 mm X 150 mm X 150 mm were also tested for the compressive strength. The tests were conducted using the crushing machine depicted in Figure 3-8. The tested cylinders and cubes are shown in Figures 3-9 and 3-10. The cubes yielded an average compressive strength of 144 MPa. The average cylinder compressive strength was found to be 110 MPa. The tensile strength of the concrete was also determined through split-cylinder testing, where it ranged between 21.2 and 23.7 MPa.

Figure 3-8: Crushing machine [15].

Figure 3-9: Cubes and cylinders before testing.

Figure 3-10: Cylinders after testing.

3.6.2 Steel reinforcement

Grade B500B steel bars, according to the British standards, were used as tensile reinforcement in the control beams. The bars had diameters of 12 and 16 mm. The actual area of the 12 mm and 16 mm bars were found to be 110.3 mm^2 and 195.8 mm^2. The properties of the steel reinforcement were provided by the manufacturer. The 12 mm bars had an average yield strength of 575 MPa, whereas the 16 mm bars had an average yield strength of 568 MPa. Two #10 steel bars were used in the compression zone of the concrete as hungers for the stirrups. In addition, steel stirrups with 10 mm diameter were used as shear reinforcement. The 10 mm bars had an average yield strength of 564 MPa. The steel used in this study had the typical value for the modulus of elasticity, 200 GPa.

3.6.3 Glass fiber reinforced polymer (GFRP) bars

Five different diameters of GFRP bars: 8-, 10-, 12-, 16-, and 20 mm were used for reinforcing the concrete beams. GFRP bars with sand-coated surfaces were used for the majority of the GFRP reinforced beams. One beam was prepared using #12 GFRP bars with ribbed surface. The sand-coated GFRP bars were manufactured and supplied by Galen in Russia, whereas the ribbed GFRP bars were supplied by Pultron Composites in UAE. The sand-coated and ribbed GFRP bars are shown in Figure 3-11. Furthermore, the tensile properties for the GFRP bars are listed in Table 3-3.

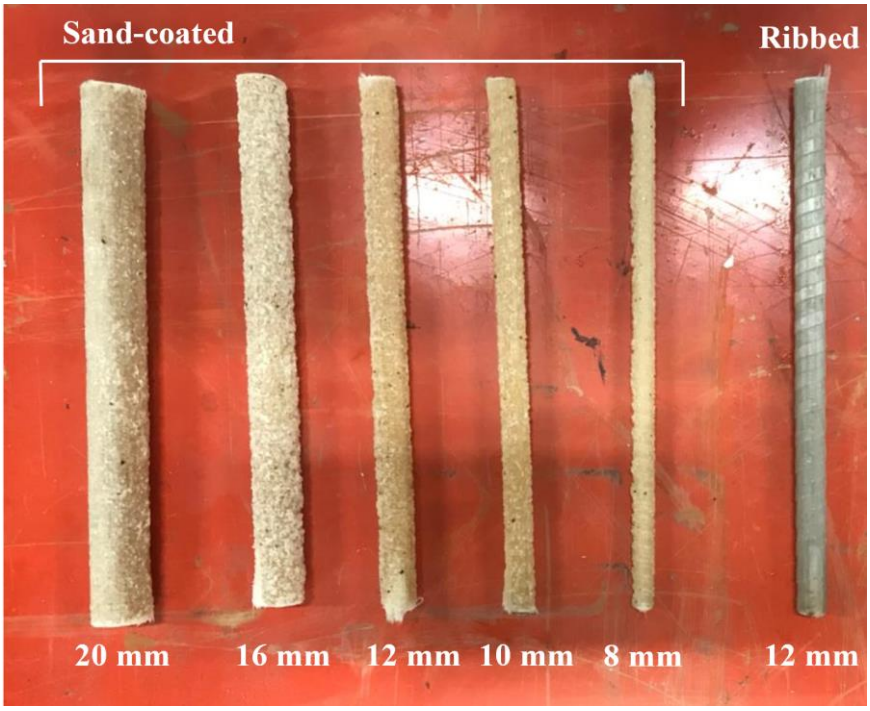

Figure 3-11: GFRP bars.

The cross-sectional area of the FRP bars was measured according to the ACI 440.3R standard [41]. A total of five bar specimens with 200 mm length were used for each bar diameter. The length of each specimen was measured three times by rotating the specimens 120 degrees for each measurement. The specimen length was then determined by taking the average of the three measurements. A cylinder was filled with water and the volume of water before and after immersing the specimen was measured. Thus, the increase in the volume of water was determined. After finding the volume and length of the five specimens, the cross-sectional areas were calculated by dividing the volume of the specimens by their length. The mean value of the cross-sectional area was then found by taking the average of the five bar specimens.

Table 3-3: Tensile properties of GFRP bars.

	Sample designation	Cross sectional area (mm^2)	Ultimate tensile stress (MPa)	Modulus of elasticity (GPa)
Sand-coated GFRP	GFRP 8	50.07	983	44.9±1.3
	GFRP 10	94.11	960	
	GFRP 12	121.20	976	
	GFRP 16	201.67	874	
	GFRP 20	325.33	779	
Ribbed GFRP	GFRP 12	99.00	823	

3.6.4 Basalt fiber reinforced polymer (BFRP) bars

In this study, the BFRP bars had 10- and 20-mm diameters (Refer to Figure 3-12) and were provided by Galen in Russia. Table 3-4 lists the tensile properties of the BFRP bars.

Table 3-4: Tensile properties of BFRP bars.

Sample designation	Cross sectional area (mm^2)	Ultimate tensile stress (MPa)	Modulus of elasticity (GPa)
BFRP 10	80.04	1028.7	42.8±1.3
BFRP 20	328.03	913	45.9±2.1

Figure 3-12: BFRP bars.

3.7. Sample Preparations

The beams were prepared by following five major steps. The reinforcement cages were first constructed using the reinforcing bars and stirrups. Strain gauges were fixed on the reinforcing bars, as shown in Figure 3-13, to capture the reinforcement strains. Then, the cages were placed in their respective formworks. Finally, the Transgulf Readymix Concrete was poured into the formworks and the beams were cured for 28 days (see Figure 3-14).

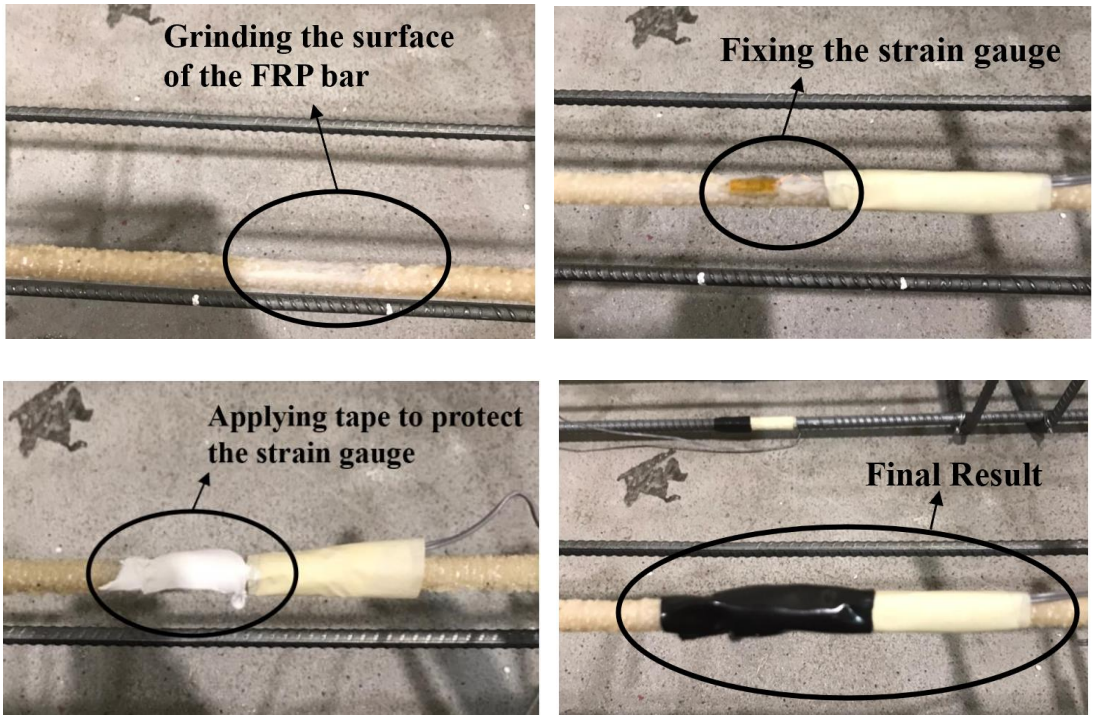

Figure 3-13: Fixing strain gauges on FRP bars.

Figure 3-14: Casting process of specimens.

3.8. Test Setup

The four-point loading setup, depicted in Figure 3-15, was used in this research to examine the flexural behavior of the UHSC beams. The load is applied through hydraulic jacks on a spreader beam, which then divides the load equally onto two points, with a 400 mm distance between them. This distance becomes the constant bending moment region, as illustrated in Figure 3-16. The testing was performed using a Universal Testing Machine (UTM), which can be seen in Figure 3-17.

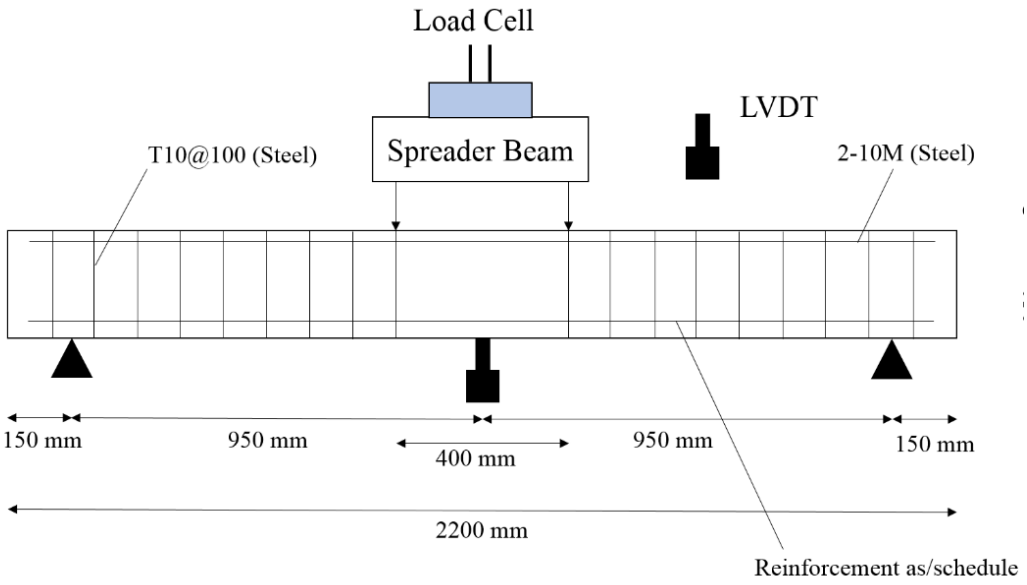

Figure 3-15: Schematic testing setup.

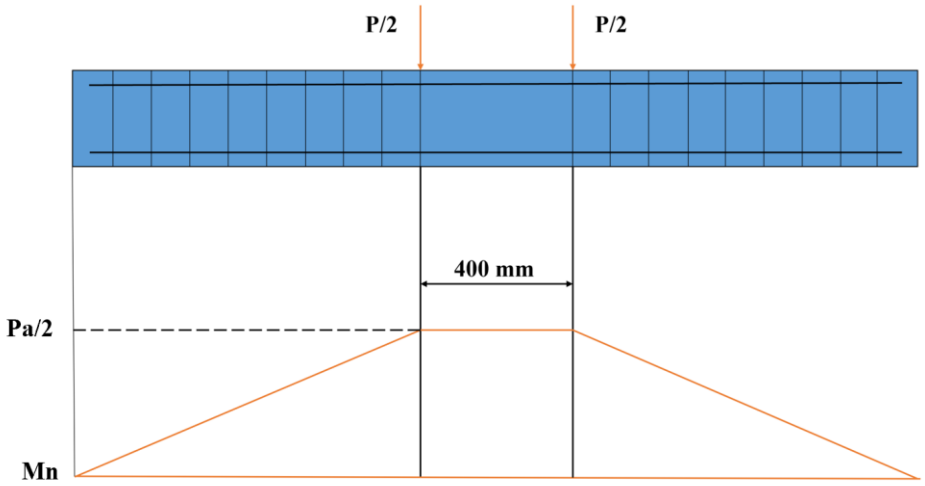

Figure 3-16: Constant moment zone.

Figure 3-17: Universal Testing Machine (UTM).

The beams had a clear span length of 1900 mm, a shear span length of 750 mm, and 150 mm overhang on each side (see Figure 3-18). Strain gauges were installed on both the concrete and the bottom reinforcing bars to measure the strain in both materials. The concrete strain gauge was placed at the midspan section, 10 mm below the top compression fibers. The reinforcement strain gauges were placed at the center of the bottom bars. A Variable Differential Transformer (LVDT) was fixed at the center of the beam from below to measure the midspan deflection. The LVDT was connected to an automatic data acquisition system to record the deflection readings continuously. The strain gauges and LVDT are shown in Figure 3-19.

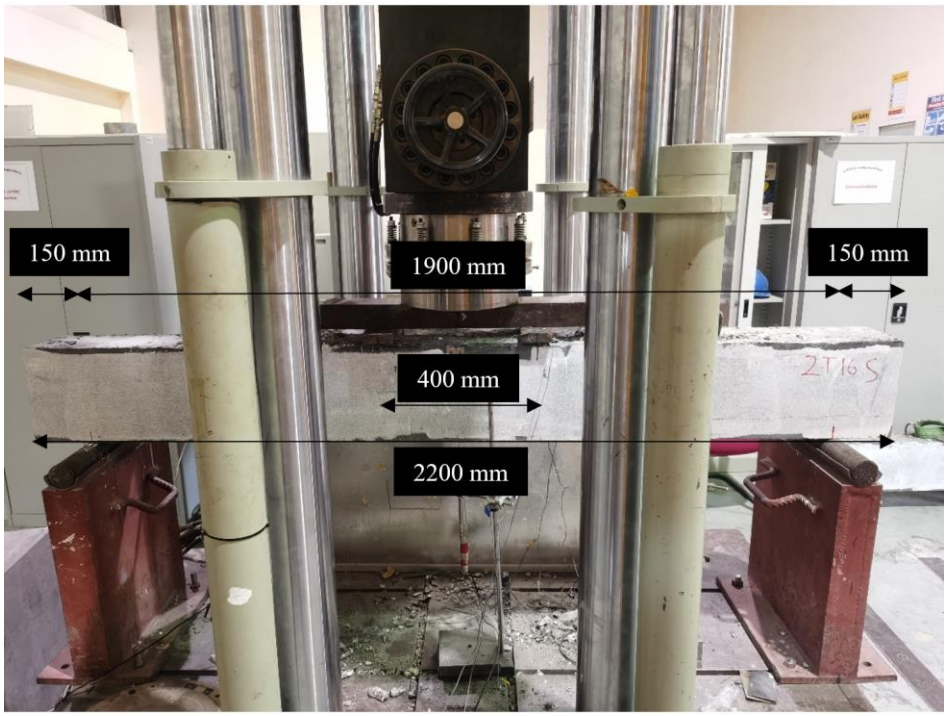

Figure 3-18: Beam's testing setup.

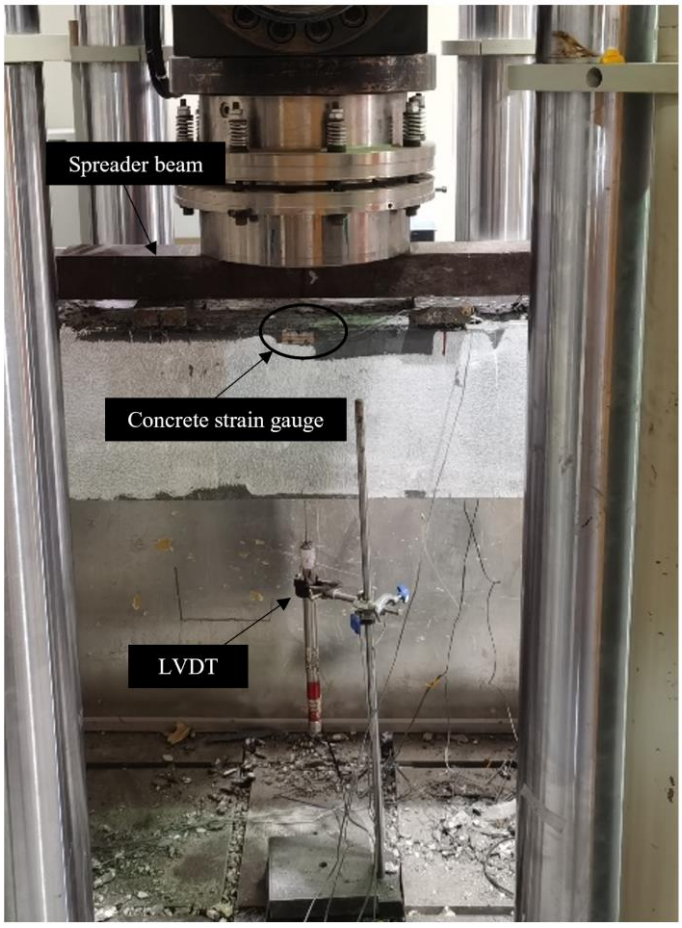

Figure 3-19: Concrete strain gauge and LVDT.

Chapter 4. Results and Analysis

This chapter presents the results of the study in terms of failure modes, load versus midspan deflection behavior, concrete and reinforcing bars strain values, and cracking patterns. The impact of using different reinforcement ratios, different reinforcement types, different number of bars, and different surface textures, are also examined and thoroughly discussed. Finally, the analytical predictions from the ACI 440 and CAN/CSA codes are verified by comparing them to the test results.

4.1. Failure Modes

The cracking patterns and failure modes of the under-reinforced beams are shown in Figure 4-1. The beams were designed to be tension-controlled and fail by the rupture of the FRP reinforcement. At first, vertical cracks appeared around the midspan region when the tensile strength of the concrete was exceeded. Cracking loads at which vertical cracks were initiated are reported in Table 4-1. As the load increased, cracks started forming near the flexural region, while the already formed cracks propagated slowly towards the compressive zone of the beams. At higher loads, new cracks started forming around the midspan and started propagating across the height of the beams. The cracks kept on propagating until the FRP bars ruptured at the region of maximum bending moment, and the beams failed. The rupture of the FRP reinforcement caused the widening of the cracks that were in the midspan region and close to the loading points. The failure occurred in an abrupt manner, without any previous warning. Nonetheless, the concrete in the compressive zone remained intact at the time of failure. The steel reinforced beams were also tension-controlled and failed due to the yielding of steel reinforcement, as shown in Figure 4-2.

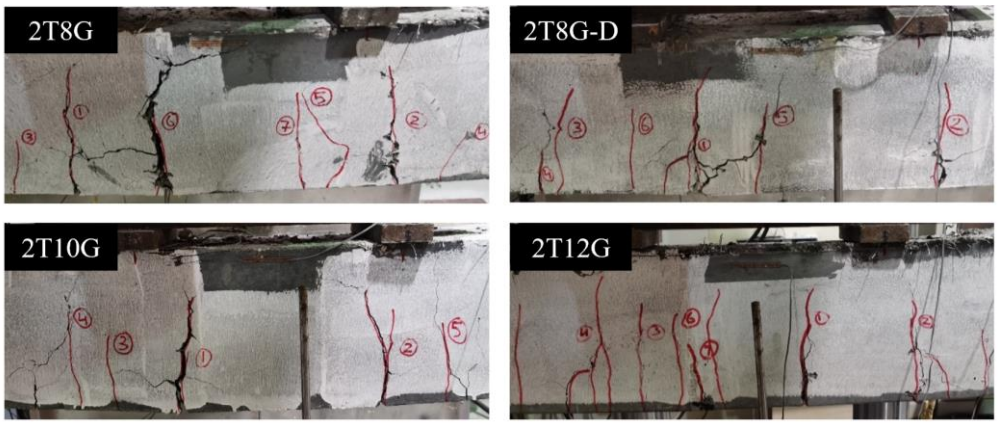

Figure 4-1: Failure modes and cracking patterns of under-reinforced beams.

Figure 4-2: Failure modes and cracking patterns of steel reinforced beams.

The over-reinforced beams were designed to be compression-controlled and fail by concrete crushing. This mode of failure, along with the cracking behavior of over-reinforced beams is depicted in Figure 4-3. The vertical cracks initially formed in the maximum bending moment region at cracking loads ranging from 28.75 kN to 31.12 kN. Similar to under-reinforced beams, new cracks started forming in the midspan region and near it. During the formation of new cracks, existing cracks started propagating towards the compressive zone of the beams. However, the propagation of the cracks in the over-reinforced beams was very slow, which resulted in lower crack depths than the under-reinforced beams at the time of failure. This shows that the bridging effect of the UHSC, which helps control crack widths and depths, is more pronounced in over-reinforced beams than in under-reinforced beams. Also, comparing the cracking behavior with HSC beams reinforced with FRP bars from previous studies [3] show that the use of UHSC yielded smaller crack depth propagations. Prior to failure, the concrete cover started crushing for the over-

reinforced beams at a loading level corresponding to the maximum load, listed in Table 4-2, for beams 2T20G and 2T20B. For beam 2T16G, the load was slightly less than the maximum load when the crushing of concrete cover started. The 2T16G and 2T20G beams experienced a drop in the load at that point, after which the beams were able to sustain additional loads until complete failure occurred. At failure, the concrete at the top surface was heavily damaged and absolutely crushed and a drop in the load was noticed. The 2T16G beam experienced the greatest amount of damage accompanied by significant widening of cracks in the midspan region.

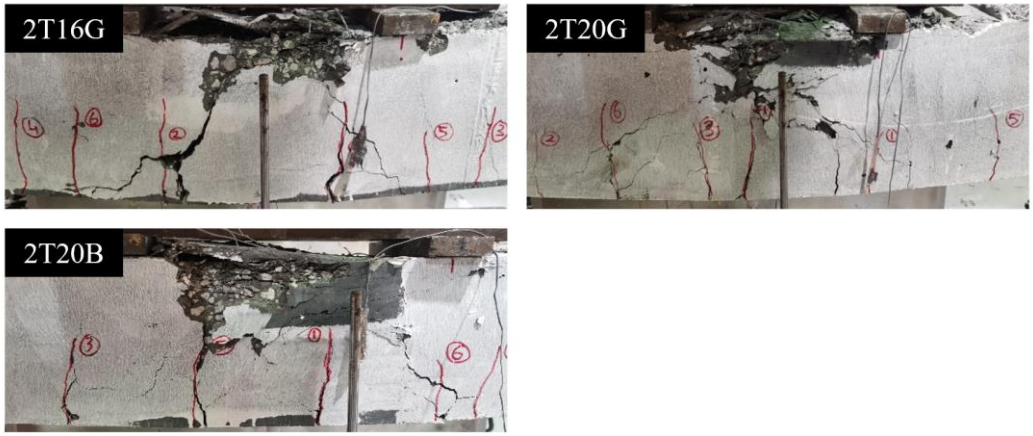

Figure 4-3: Failure modes and cracking patterns of over-reinforced beams.

The 3T10G beam was originally designed to have a tensile failure. However, the No. 10 GFRP bars had larger cross-sectional areas than expected, which caused the beam to fall in the balanced region. Thus, this beam and its duplicate experienced both concrete crushing and FRP rupture simultaneously. It can be seen from Figure 4-4 that the concrete in the compressive zone was not severely damaged, unlike the case of over-reinforced beams. This is because the bars ruptured while the concrete was crushing, and the beams failed immediately. However, there were clear signs of crushing of the concrete cover before total failure occurred, which proves that this type of beam did not exhibit brittle failure like the tension-controlled beams. The concrete cover crushed at an ultimate load of 133.13 kN and 127.03 kN for the 3T10G and 3T10G-D beams, respectively. The beams were able to carry further load up until the FRP reinforcing bars ruptured, and the beams failed instantaneously. Failure happened at a loading level of 125.95 kN and 122.10 kN for the 3T10G and 3T10G-D beams, respectively. In addition, widening of existing cracks also occurred at the time of failure.

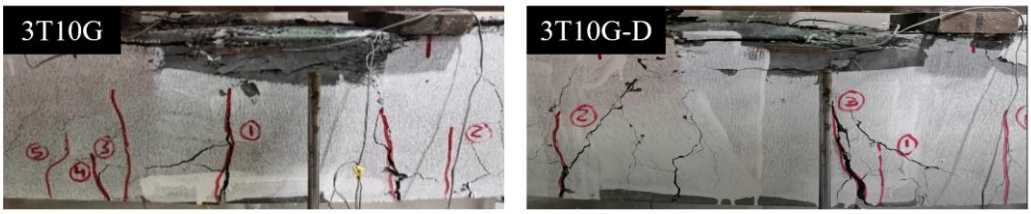

Figure 4-4: Failure modes and cracking patterns of the 3T10G beam.

4.2. Load-Midspan Deflection Behavior

Figure 4-5 shows the load versus midspan deflection behavior of the UHSC beams. The beams were grouped based on the main parameters investigated in this study: reinforcement ratio, number of bars, and type of reinforcement.

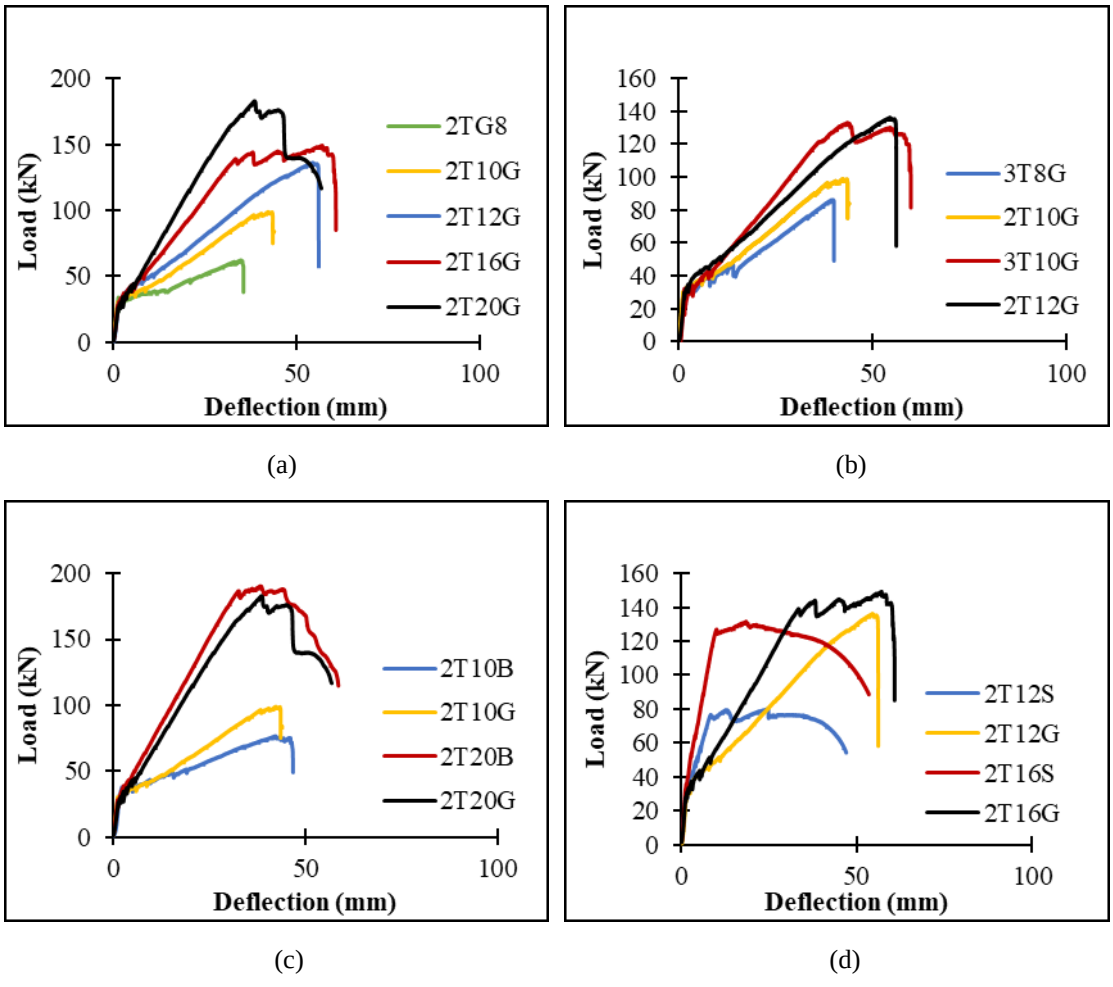

Figure 4-5: Load vs. deflection curves for (a) different reinforcement ratios; (b) different number of bars; (c) BFRP vs GFRP reinforced beams; (d) steel vs GFRP reinforced beams.

All the tested specimens exhibited a bilinear behavior up until failure. Previous studies on FRP reinforced beams developed with NSC and HSC also reported a

bilinear load-midspan deflection behavior. For the under-reinforced beams, failure occurred due to the rupture of FRP reinforcement. Those beams showed a linear elastic behavior and failed instantaneously once they reached the ultimate load. On the other hand, the over-reinforced beams (2T16G, 2T20G, and 2T20B) showed some amount of ductility and carried additional loads even after reaching the ultimate load level. Similar behavior was observed for beam 3T10G. This supports the ACI 440 and CAN/CSA recommendations of designing FRP reinforced beams to be compression-controlled to improve the ductility of such type of beams. Similar findings were also reported by Golston et al. [36] for both under-reinforced and over-reinforced beams made with UHSC. Table 4-2 presents a summary of the flexural test results including the ultimate moment capacity, the maximum midspan deflection, the cracking moment, and the failure mode of each tested specimen.

Table 4-1: Summary of flexural test results.

Beam	Max Load (kN)	Moment Capacity (kN.m)	Max. Deflection (mm)	First Cracking Load (kN)	Cracking Moment (kN.m)	Failure Mode
2T8G	62.36	23.39	35.25	34.16	12.810	FRP Rupture
2T8G-D	52.41	19.65	32.63	29.49	11.060	FRP Rupture
2T10G	98.99	37.12	43.32	30.48	11.430	FRP Rupture
2T12G	136.33	51.13	55.82	29.79	11.170	FRP Rupture
2T16G	149.34	56.00	59.67	31.12	11.670	Concrete Crushing
2T20G	182.92	68.60	46.38	28.75	10.780	Concrete Crushing
3T8G	86.27	32.35	39.78	31.33	11.750	FRP Rupture
3T10G	133.13	49.92	59.47	32.35	12.130	CC and FR*
3T10G-D	127.03	47.64	55.27	28.99	10.870	CC and FR*
2T12GR	112.58	42.22	46.17	28.75	10.780	FRP Rupture
2T10B	76.61	28.73	46.40	31.23	11.710	FRP Rupture
2T20B	190.44	71.41	44.57	29.68	11.130	Concrete Crushing
2T12S	80.12	30.05	35.89	33.17	12.440	Steel Yielding
2T12S-D	84.08	31.53	22.80	29.44	11.040	Steel Yielding
2T16S	131.66	49.37	40.59	35.97	13.490	Steel Yielding

*Beams failed by concrete crushing and FRP rupture simultaneously.

4.3. Reinforcement and Concrete Strain

Strain gauges were fixed at the top surface of the concrete, as well as at the middle of the reinforcing bars to capture the strain values at the desired locations. Table 4-2 lists the strain readings in the concrete and reinforcement at failure. The strain at the ultimate load in the concrete and reinforcing bars of few specimens could not be established. This is because the strain gauges were damaged prior to achieving that loading level. Hence, a linear regression analysis was performed to evaluate the

strains at the ultimate load levels by assuming that the post-cracking strain behavior was linear. The same approach was followed by Goldston et al. [36].

Table 4-2: Reinforcement and concrete strain values at ultimate load.

	Moment (kN.m)	Concrete Strain	Reinforcement Strain
2T8G	23.39	N/A*	0.023
2T10G	37.12	0.0036	0.021
2T12G	51.13	0.0033	0.022[a]
2T16G	56.00	N/A*	0.016[a]
2T20G	68.60	0.003[a]	0.015
3T8G	32.35	0.0026	0.022[a]
3T10G	49.92	0.0037 [a]	0.023
2T12GR	42.22	N/A*	0.021[a]
2T10B	28.73	0.0033[a]	0.023
2T20B	71.41	0.0038	0.017
2T12S	30.05	0.0044	0.014
2T16S	49.37	N/A*	0.022

[a] Linear regression analysis was performed to evaluate the strain at the ultimate load

*Due to the damage of strain gauge

The moment-strain behaviour in the concrete and reinforcing bars is displayed in Figure 4-6. All the FRP reinforced beams, designed as tension-controlled, reported average reinforcement strains very close to the rupture strains. The strain values in these beams ranged between 0.021 and 0.023. On the other hand, the average reinforcement strains for the over-reinforced beams (2T16G, 2T20G, and 2T20B) varied between 0.015 and 0.017, which is around 85% of the rupture strain. This supports the concrete crushing failure mode that was exhibited by those beams. The 2T12S and 2T16S beams had average reinforcement strains of 0.014 and 0.022, respectively, which is well beyond the yield strain of the steel bars (0.0029).

For the UHSC beams, the concrete strain values of the FRP reinforced beams varied between 0.0026 and 0.0038 at the ultimate load level. The concrete strain values were found to be in the range of 0.0025 - 0.0033 for NSC beams and 0.0028 – 0.0038 for HSC beams [3]. This shows that increasing the concrete strength had a negligible effect on the concrete strain values of FRP reinforced beams at ultimate load levels. A similar conclusion was reported by Goldston et al. [36] for HSC and UHSC beams. Despite the 2T20G beam being designed as compression-controlled, it reported a relatively low concrete strain value of 0.003. However, it must be noted that, unlike

the under-reinforced beams, the over-reinforced beams did not fail at the ultimate load, and kept on carrying additional loads, until the concrete in the compression zone was disintegrated. This means that the 2T20G beam failed at a larger concrete compressive strain than 0.003. However, the exact value was not established due to the damage of the strain gauge. Likewise, the 2T20B beam had an average concrete strain of 0.0038, but the ultimate strain was larger than that value. The steel reinforced beam, 2T12S, reported an ultimate concrete compressive strain of 0.0044. The 3T10G beam had a relatively high concrete strain value of 0.0037 and an average reinforcement strain of 0.023, which is very close to the rupture strain. This proves that this beam experienced both concrete crushing and FRP reinforcement rupture at failure.

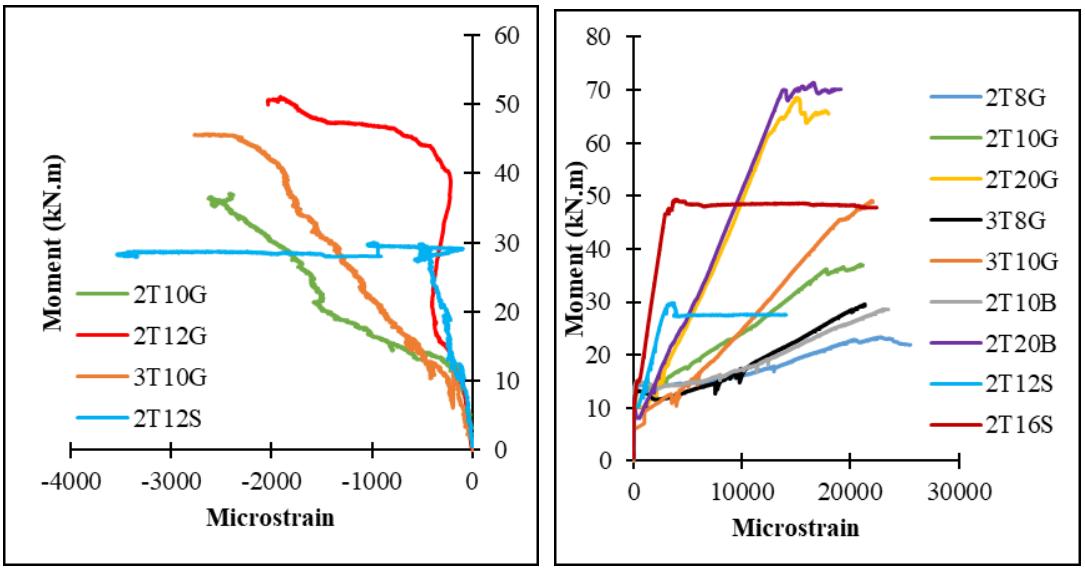

Figure 4-6: Recorded strains in longitudinal reinforcement and concrete.

4.4. Duplicated Beams

Three beams from the experimental program were duplicated to improve the accuracy and reliability of the results. The 2T8G, 3T10G, and 2T12S beams were cast again and tested without varying any of the parameters. As shown in Figure 4-7, the moment versus deflection behavior for the duplicated FRP reinforced beams (2T8G-D and 3T10G-D) were almost identical to the original beams with minor discrepancies. The discrepancies in the values were within acceptable limits and can occur due to numerous reasons, such as variability in the material properties of the concrete or the reinforcement. The results for the two steel-reinforced beams were also comparable.

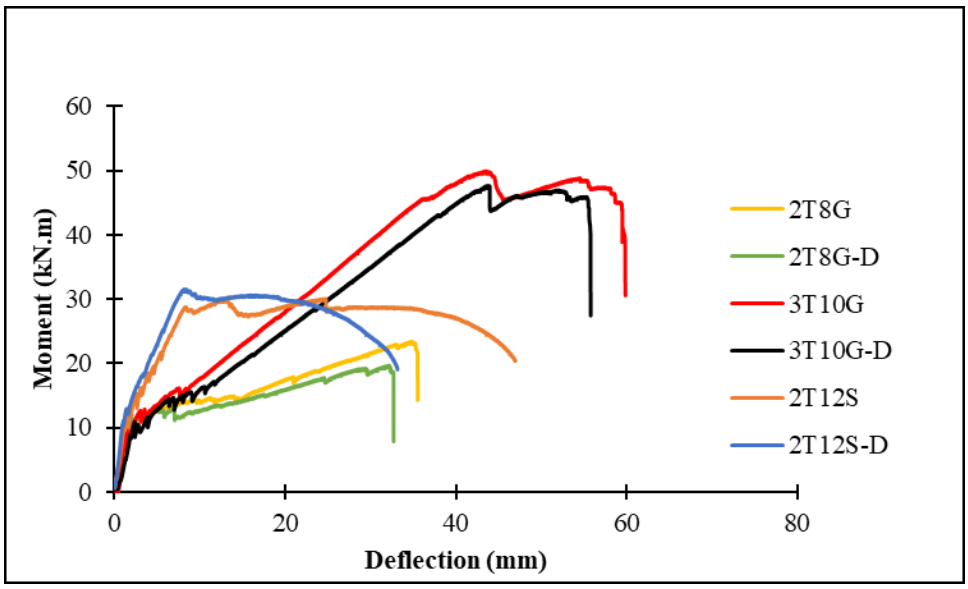

Figure 4-7: Moment vs deflection curve for the duplicated beams.

4.5. Influence of Reinforcement Ratio

The impact of reinforcement ratio on the flexural behavior was investigated by varying the GFRP reinforcement ratio between 0.0026% and 0.0176%. Increasing the reinforcement ratio led to an increase in the flexural capacities of the GFRP reinforced beams, as shown in Figure 4-8. The increase was not proportional, which agrees well with the ACI code equation for evaluating the moment capacity of FRP reinforced beams. For the under-reinforced beams, the moment capacity increased by 58.7% for an 89.4% increase in the reinforcement ratio between beams 2T8G and 2T10G and increased by 37.7% when the reinforcement ratio increased 29.2% between beams 2T10G and 2T12G. In the case of over-reinforced beams, a 63.1% increase in the reinforcement ratio between beams 2T16G and 2T20G led to a 22.5% increase in the moment capacity.

Increasing the reinforcement ratio by 67.9% for the 2T12G and 2T16G beams resulted in a change in the failure mode from FRP rupture to concrete crushing and a 9.52% increase in the flexural capacity. According to Goldston et al. [36], increasing the GFRP ratio from 0.5% to 1.0% led to a 120% increase in the load-carrying capacity of HSC beams and up to 158% increase in that of UHSC beams. The authors attributed the significant increase in the load-carrying capacity to the change in failure mode from GFRP rupture to concrete crushing. Likewise, Adam et al. [25] reported around 57% increase in the ultimate capacity of HSC beams reinforced with GFRP

bars by using 1.7 times the reinforcement ratio and changing the mode of failure. However, changing the failure mode in this study from tensile to compressive failure was not very effective in significantly increasing the ultimate moment capacity.

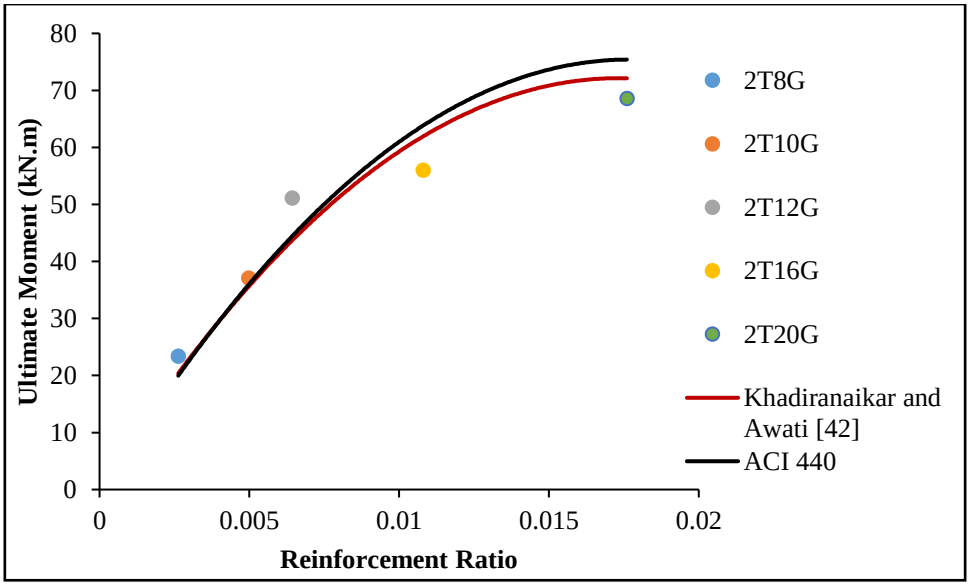

Figure 4-8: Effect of reinforcement ratio on the ultimate moment of UHSC beams.

To understand the effect of the concrete strength on the flexural behavior of FRP reinforced beams, the tested specimens from this experimental program were compared with FRP reinforced beams developed with HSC and NSC from a previous study [3]. The NSC and HSC beams were also found to follow the ACI 440 trend for the flexural capacity, where the increase in reinforcement ratio led to a nonproportional increase in the flexural capacity. However, the ACI 440 equation predicted well the moment capacity of beams with high reinforcement ratios in the case of HSC and NSC beams, unlike the case of UHSC beams. This can be attributed to the stress block parameters. Khadiranaikar and Awati proposed a modification to the stress block parameters for concrete strengths up to 120 MPa when designing flexural members. The authors stated that the parameters α and β are to be considered as 0.85 each for a concrete compressive strength of 20 MPa, and are to be reduced by 0.02 and 0.04, respectively, for every 20 MPa increase in strength. Also, the minimum value for α and β should be taken as 0.75 and as 0.67, respectively [42]. By applying this to the beams in this study, the ACI 440 equation yielded somewhat better predictions of the flexural capacity for over-reinforced beams (see Figure 4-8). This shows that the ACI 440 equation for flexural capacity needs to be revised and

more research must be conducted on the stress block parameters to account for concrete strengths greater than 120 MPa.

The effect of reinforcement ratio on the moment versus midspan deflection behavior is displayed in Figure 4-9. Irrespective of the reinforcement ratio, all the beams exhibited similar stiffnesses and behavior before cracking. Then, there was a reduction in the stiffness once cracking occurred. The post cracking stiffness increased with the increasing GFRP reinforcement ratio. In other words, beams with higher reinforcement ratios, and thus higher bending stiffnesses, had smaller midspan deflection values at the same load level. In addition, the maximum midspan deflection increased with increasing the GFRP reinforcement ratio for the under-reinforced beams. On the other hand, increasing the FRP reinforcement ratio in over-reinforced beams reduced the maximum midspan deflection.

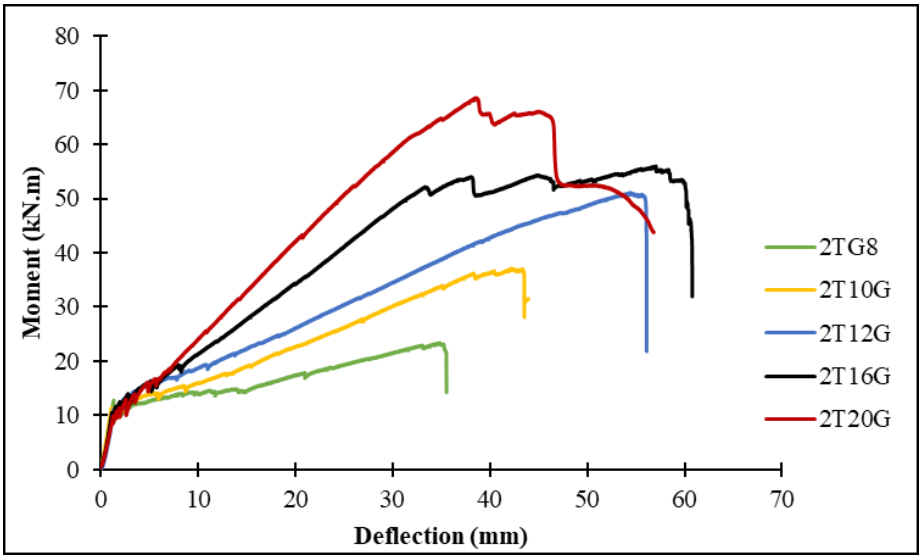

Figure 4-9: Moment vs. deflection curve for different reinforcement ratios.

Since there is no clear definition of the service load in the design codes, some studies considered the service load to be at around 30% of the nominal moment capacity. Hence, the deflection values were considered at two load levels, $0.3M_n$ and $0.67M_n$, in this study. The deflection values at $0.3M_n$ and $0.67M_n$ were plotted against ρ_f/ρ_{fb}, as shown in Figure 4-10. At a loading level of $0.3M_n$, the deflection values increased with an increasing ρ_f/ρ_{fb}. Different findings were reported by El-Nemr et al. [4] who found that increasing the ρ_f/ρ_{fb} ratio helped in decreasing the deflection values for NSC and HSC beams with GFRP reinforcement. This shows that care must

be taken when designing UHSC beams with high FRP reinforcement ratios so that they meet serviceability limit states and do not exhibit large service deflections. At a loading level of $0.67M_n$, the deflection values followed a different trend. As the ρ_f/ρ_{fb} ratio increased, the midspan deflection for the under-reinforced beams increased too. Then, the midspan deflections decreased significantly for the over-reinforced beams (2T16G and 2T20G). Both the over-reinforced beams had a somewhat similar midspan deflection value at that loading level.

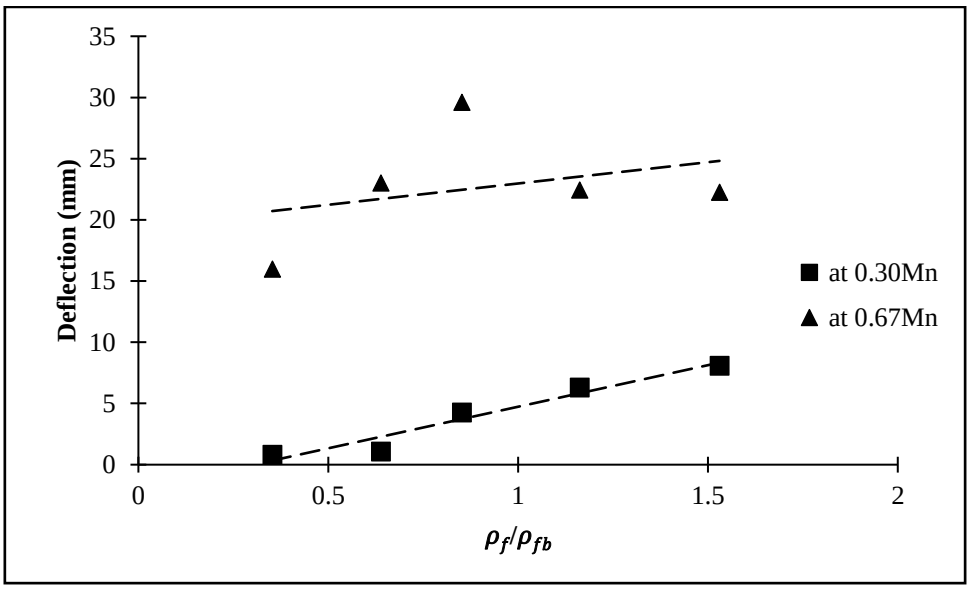

Figure 4-10: Deflection versus ρ_f/ρ_{fb}.

The cracking moment of the GFRP reinforced beams ranged between 10.78 kN.m and 12.81 kN.m with an average value of 11.49 kN.m. This value is around 27% of the average flexural capacity. Since the cracking moment depends on the modulus of rupture, which is a function of the concrete compressive strength, increasing the reinforcement ratio had a negligible effect on the cracking moment of the tested beams. The same thing was reported by Abed et al. [3] for NSC and HSC beams. All the UHSC beams exhibited the traditional flexural cracking response (see Figures 4-1 and 4-3). Increasing the reinforcement ratio led to the mitigation of the crack width at failure for the under-reinforced beams (2T8G, 2T10G, and 2T12G). Likewise, increasing the GFRP ratio between beams 2T16G and 2T20G resulted in less damage to the concrete in the compressive zone and narrower cracks.

The reinforcement ratio also impacted the GFRP strain values. As shown in Figure 4-6, the 2T8G beam showed sharp increases in the bar strain as compared to the 2T10G

beam. This is because beams with lower reinforcement ratios have poor energy absorption capacities and experience abrupt changes in their stiffness at cracking. Similarly, the reinforcement strain in the 2T10G beam rapidly increased as compared to the 2T20G beam. It can also be observed that the average bar strain decreased from 0.016 to 0.015, as the reinforcement ratio increased between beams 2T16G and 2T20G.

The neutral axis was located at the mid height of the beam section prior to cracking and it then decreased significantly just after cracking. As shown in Figure 4-11, the neutral axis depth was found to be 30 mm and 33 mm for the 2T10G and 2T20G beams, respectively, at the ultimate load levels. This is expected as increasing the reinforcement ratio requires a larger concrete compressive block to balance the greater tensile forces.

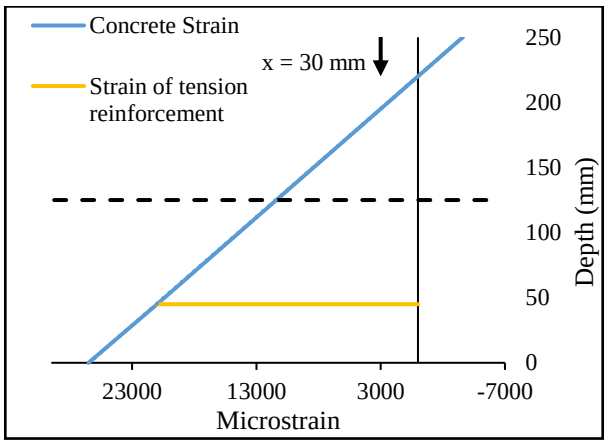

(a)

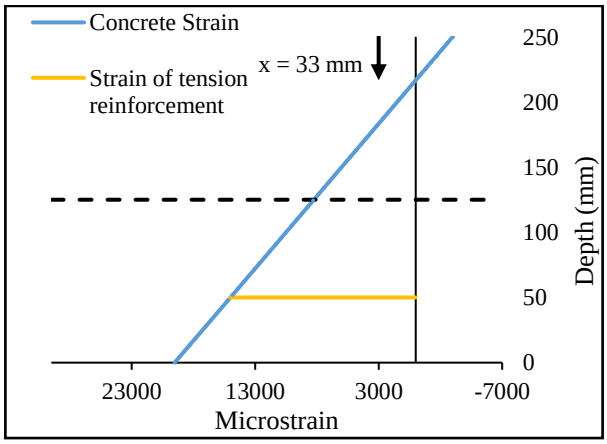

(b)

Figure 4-11: Neutral axis depth at ultimate loads for the (a) 2T10G (b) 2T20G beams.

4.6. Influence of Number of Bars

To investigate the effect of the number of bars on the flexural behavior, beams with same axial stiffnesses and reinforcement ratios, but different number of tensile bars (2 and 3 bars) were compared against each other (3T8G vs. 2T10G and 3T10G vs. 2T12G). It must be noted, however, that the 2T10G and the 3T10G beams had slightly higher bending stiffnesses than the 3T8G and 2T12G beams, respectively (Refer to Table 3-1). The 2T12G beam had a brittle failure due to the rupture of GFRP reinforcement, whereas the 3T10G beam failed due to both concrete crushing and FRP rupture. Hence, the moment vs. deflection response for the two beams were different, as the 3T10G beam showed some signs of ductility before failing (Refer to Figure 4-12).

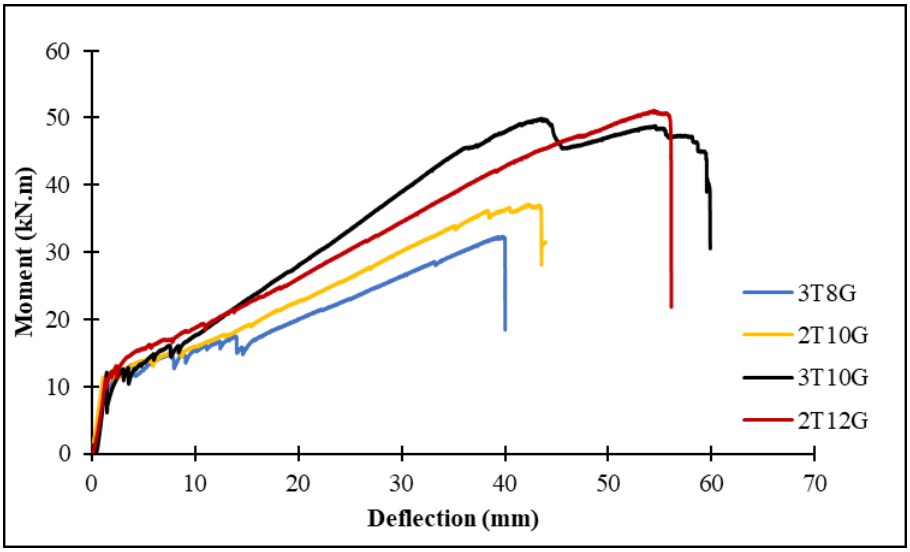

Figure 4-12: Moment vs. deflection curve for different number of longitudinal bars.

However, the effect of number of bars on the flexural capacity and midspan deflection of the 3T10G and 2T12G beams was insignificant in spite of the difference in failure mode. On the other hand, the 2T10G beam had a larger flexural capacity and maximum midspan deflection than the 3T8G beam by 14.7% and 8.9%, respectively. Abed et al. [3] also reported slightly larger midspan deflection values for NSC and HSC beams reinforced with two bars as compared to those reinforced with three bars.

Moreover, the first cracking moments were not notably affected by the number of longitudinal bars. The cracking moment increased in the range of 2.8% to 8.6% when three longitudinal bars were used (3T8G and 3T10G). According to the ACI 440.1R-

15 equation, the crack width of the beam should decrease when the spacing between the bars is reduced. This can be seen in Figure 4-1, as the 3T8G beam had smaller crack width in the midspan region as compared to the 2T10G beam at the failure load. However, the 3T8G beam had deeper propagation of cracks as compared to the 2T10G beam. The 3T8G beam also had larger increases in the reinforcement strain as compared to the 2T10G beam, as shown in Figure 4-6. This can also be attributed to the smaller reinforcement area of the 3T8G beam.

4.7. Influence of Reinforcement Type

The beams were reinforced with three different types of flexural reinforcement: GFRP, BFRP, and steel. The first section compares GFRP and BFRP reinforced beams with equal reinforcement ratios. The second section discusses the differences in the flexural behavior between the GFRP and steel reinforced beams.

4.7.1 BFRP vs. GFRP reinforced beams

The moment versus deflection curves for the BFRP and GFRP reinforced beams were plotted in Figure 4-13. Signs of initial cracking at the midspan were evident at cracking loads ranging between 28.75 kN and 31.23 kN for the four beams. Thus, it can be concluded that the first cracking moment was not influenced by the type of FRP reinforcement used. The 2T10G beam reported higher bending stiffness than the 2T10B beam. This is because No. 10 GFRP bars had larger modulus of elasticity than their BFRP counterparts (Refer to Tables 3-3 and 3-4). Likewise, the 2T20B beam showed greater post cracking stiffness than the 2T20G beam due to the larger modulus of elasticity of the No. 20 BFRP bars. In addition, the 2T20G and 2T20B beams had similar flexural capacities, but an increase of 29.2% in the flexural capacity was recorded for the 2T10G beam as compared to the 2T10B beam. There were also minor differences in the cracking patterns, failure modes, and midspan deflections between the GFRP and BFRP reinforced beams.

It can be seen from Table 4-2 that the 2T20B beam had a larger concrete strain (0.0038) at the top compression fibers than the 2T20G beam (0.003). However, both the GFRP and BFRP bars in the over-reinforced beams achieved around 85% of their rupture strain. The 2T10G and 2T10B beams had concrete strains of 0.0036 and 0.0033, respectively, and bar strains very close to the rupture strains. In addition, the No. 10 BFRP bars had larger increases in the post cracking reinforcement strains than

the GFRP bars, but the over-reinforced beams (2T20B and 2T20G) exhibited almost identical moment-reinforcement strains behavior (Refer to Figure 4-6). In general, the GFRP and BFRP reinforced beams showed similar flexural behavior. This shows that BFRP bars can be used as alternatives to more traditional FRP reinforcement like the GFRP bars, as they provide comparable behavior in flexure.

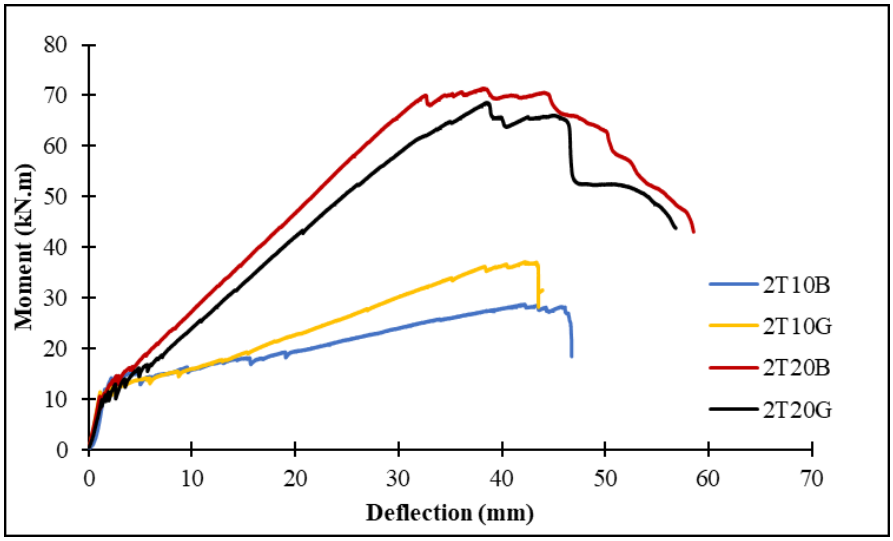

Figure 4-13: Moment vs. deflection curve for BFRP vs. GFRP reinforced beams.

4.7.2 Steel vs. GFRP reinforced beams

It is evident from Figure 4-14 that the use of GFRP reinforcement improved the flexural capacity as compared to the use of steel bars. The percentage increase in the ultimate moment capacity was found to be 70.15% for the 2T12G beam and 13.43% for the 2T16G beam as compared to the 2T12S and 2T16S beams, respectively. The significant improvement in the flexural capacity, especially for the under-reinforced beams, is due to the much higher tensile strength of the FRP bars as compared to that of steel bars. However, the steel reinforced beams reported smaller midspan deflections than the GFRP reinforced beams. Also, the steel reinforced beams showed a much higher post cracking stiffness than the GFRP reinforced beams. This is expected due to the low modulus of elasticity of the GFRP reinforcement. In addition, the steel reinforced beams reported higher cracking moments than their equivalent GFRP reinforced beams.

The 2T12S beam exhibited better ductility than the 2T12G beam. The enhanced ductility of the steel reinforced beam is also noted through the concrete strain values. At ultimate level, the 2T12S beam had attained a concrete strain value of 0.0044,

whereas the 2T12G beam had a strain value equal to 0.0033. This also indicates that using UHSC can significantly improve the concrete strain to values greater than 0.003, which is usually obtained with conventional concrete. On the other hand, the 2T16G beam displayed major inelastic deformations and ductility prior to failure, similar to the 2T16S beam.

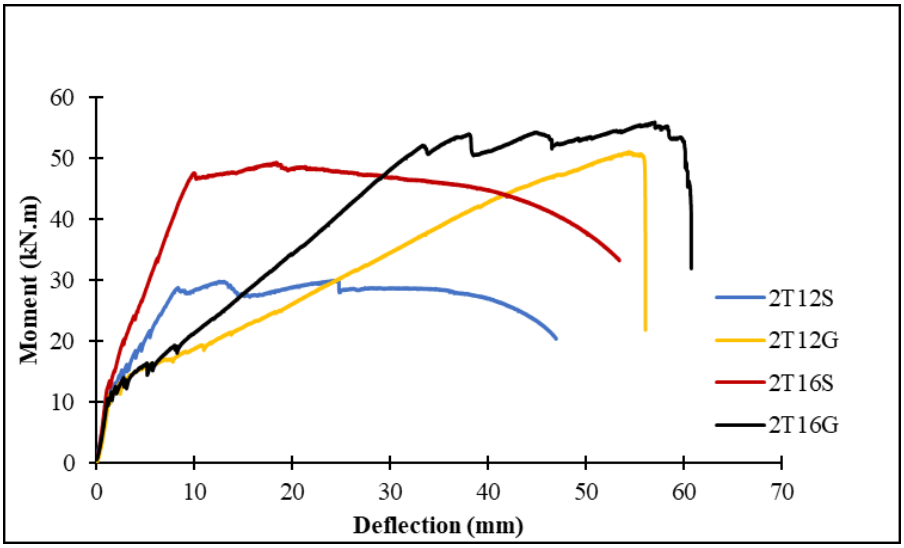

Figure 4-14: Moment vs. deflection curve for steel vs. GFRP reinforced beams.

4.8. Influence of Surface Texture

Ribbed and sand-coated GFRP bars with 12 mm diameters were used as tensile reinforcement. It is evident from Figure 4-15 that the two beams had the same post cracking slope, and hence; the same bending stiffness. This is due to the similarity in the area and modulus of elasticity of the two types of bars. However, the flexural capacity increased by around 21%, when sand-coated GFRP bars were used rather than ribbed ones. This is because the tensile strength of the sand-coated GFRP bars (976 MPa) is greater than the tensile strength of the ribbed GFRP bars (823 MPa). The midspan deflection value for the 2T12G beam (55.82 mm) was accordingly higher than that of the 2T12GR beam (46.17 mm) as shown in Figure 4-15.

The cracking behavior of the two beams can be seen in Figure 4-1. Both beams reported very similar first cracking moments. Nonetheless, the beam with sand-coated GFRP bars showed an enhanced cracking response with much greater number of cracks and smaller crack spacing as compared to the beam with ribbed GFRP bars.

Similar behavior was reported by El-Nemr et al. [4] due to the better bond characteristics of the sand-coated GFRP bars.

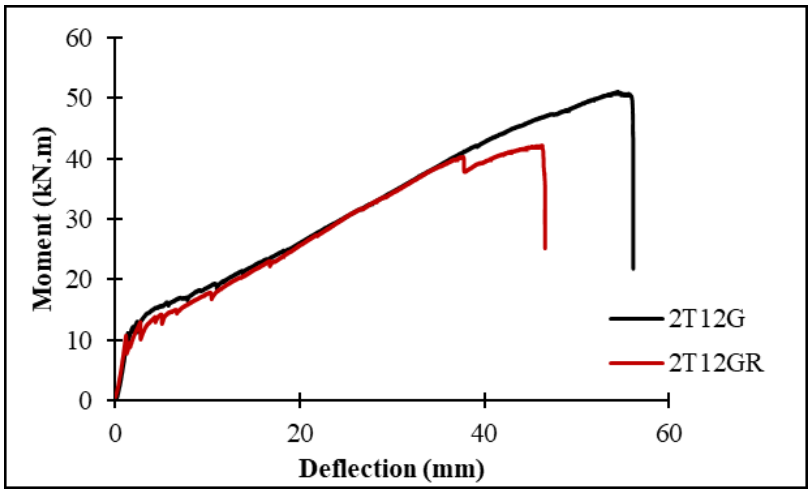

Figure 4-15: Moment vs. deflection curve for different GFRP surface textures.

4.9. Analytical Predictions

In this section, the experimental results for the cracking moment, ultimate capacity and midspan deflection are compared with predicted values obtained using the ACI 440.1R-15 and CAN/CSA S806-12 codes.

4.9.1 Cracking moment

The experimental and predicted cracking moments are provided in Table 4-3. The experimental values ranged between 10.78 kN.m and 13.49 kN.m, with an average value of 11.62 kN.m. Both the ACI and CSA predicted values were in good agreement with the experimental results. For the ACI 440 code, the ratio of experimental to predicted cracking moments had an average value of 0.93 ± 0.06. The CAN/CSA S806 yielded slightly better predictions with an average value of 0.96 and a standard deviation of 0.06. In general, both the equations overestimated the cracking moments of the FRP reinforced beams. El-Nemr et al. [4] also reported better predictions when the CAN/CSA S806 equation was used for NSC and HSC beams, due to its smaller modulus of rupture value.

Abed et al. [3] found that the ACI 440 code equation underestimated the cracking moments of NSC beams with an average experimental to predicted ratio of 1.05, whereas it overestimated the cracking moments of HSC beams with an average ratio of 0.98. The results from this study show that the ACI 440 code further overestimated

the cracking moment of UHSC beams with an average ratio of 0.93. Thus, the equation needs to be modified for beams developed with higher concrete strengths as it yields unconservative values.

Table 4-3: Experimental and predicted cracking moments.

Sr #	Beam	Exp Mcr	Mcr Exp/Pred ACI 440.1R	Mcr Exp/Pred CAN/CSA S806
1	2T8G	12.810	1.02	1.06
2	2T8G-D	11.060	0.88	0.91
3	2T10G	11.430	0.91	0.94
4	2T12G	11.170	0.89	0.92
5	2T16G	11.670	0.93	0.96
6	2T20G	10.780	0.86	0.89
7	3T8G	11.750	0.94	0.97
8	3T10G	12.130	0.97	1.00
9	3T10G-D	10.870	0.87	0.90
10	2T12GR	10.780	0.86	0.89
11	2T10B	11.710	0.93	0.97
12	2T20B	11.130	0.89	0.92
13	2T12S	12.440	0.99	1.03
14	2T12S-D	11.040	0.88	0.91
15	2T16S	13.490	1.08	1.11
	Average	11.62	0.93	0.96
	Standard Deviation		0.06	0.06

4.9.2 Flexural capacity

As discussed in Chapter 3, the ACI 440.1R-15 equation for finding the flexural capacity is used with the assumption that the specimens fail at an ultimate compressive strain of 0.003. Thus, the flexural capacities of the UHSC beams were calculated accordingly and are summarized in Table 4-4. On average, the ratio of experimental to predicted moment capacity was found to be 1.05±0.14 for all the tested beams. The ACI 440 equation underestimated the moment capacity of the GFRP reinforced beams, that were designed as tension-controlled. On the other hand, the equation overestimated the capacity of the BFRP reinforced beams (2T10B and 2T20B), as well as the GFRP over-reinforced beams (2T16G and 2T20G). However, by multiplying the nominal capacities of those four beams with the reduction factors, the predicted results become conservative and acceptable (Refer to Figure 3-2). Furthermore, the ACI 318 equation provided conservative results for the steel reinforced beams, where the ratio of experimental to predicted moments ranged between 1.13 and 1.24.

Table 4-4: Experimental and predicted ultimate moments.

Sr #	Beam	Exp Mn	Predicted Mn	Mn Exp/Pred
			ε_{cu} = 0.003	ε_{cu} = 0.003
1	2T8G	23.39	19.48	1.20
2	2T8G-D	19.65	19.48	1.01
3	2T10G	37.12	35.48	1.05
4	2T12G	51.13	46.31	1.10
5	2T16G	56.00	62.61	0.89
6	2T20G	68.60	75.66	0.91
7	3T8G	32.35	29.22	1.11
8	3T10G	49.92	53.22	0.94
9	3T10G-D	47.64	53.22	0.90
10	2T12GR	42.22	31.78	1.33
11	2T10B	28.73	32.54	0.88
12	2T20B	71.41	76.61	0.93
13	2T12S	30.05	25.41	1.18
14	2T12S-D	31.53	25.41	1.24
15	2T16S	49.37	43.53	1.13
	Average			1.05
	Standard Deviation			0.14

4.9.3 Deflection

Figure 4-16 compares the experimental and predicted moment-deflection responses of the tested beams. In general, both codes underestimated the maximum deflections of the FRP reinforced beams. This is even more pronounced in over-reinforced specimens, as the design codes do not consider the additional ductility that the beams gained. However, the model provided by the CSA better predicted the deflection compared to the ACI 440, irrespective of the reinforcement ratio. A similar conclusion was reported by Goldston et al. [36].

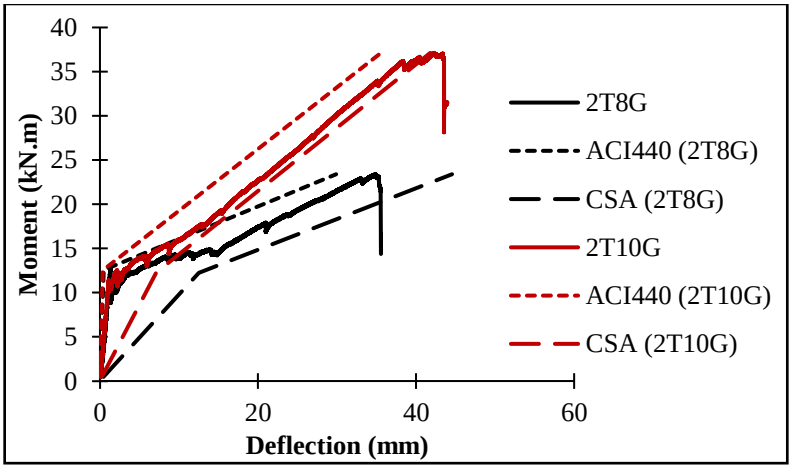

(a)

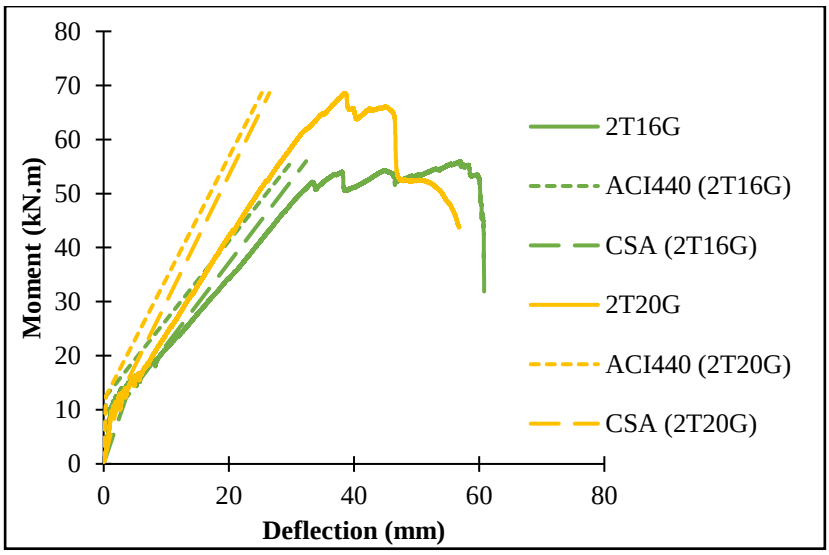
Moment (kN.m)
Deflection (mm)
0
10
20
30
40
50
60
70
80
0
20
40
60
80
2T16G
ACI440 (2T16G)
CSA (2T16G)
2T20G
ACI440 (2T20G)
CSA (2T20G)

(b)

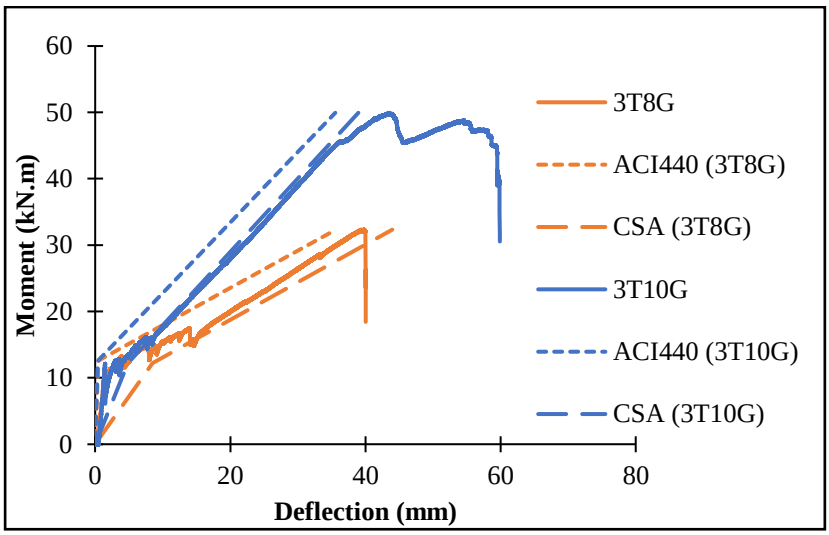
Moment (kN.m)
Deflection (mm)
0
10
20
30
40
50
60
0
20
40
60
80
3T8G
ACI440 (3T8G)
CSA (3T8G)
3T10G
ACI440 (3T10G)
CSA (3T10G)

(c)

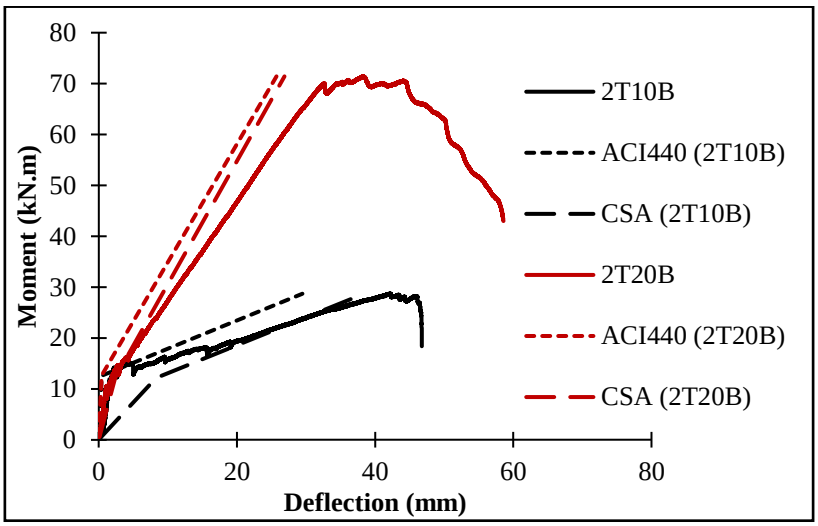
Moment (kN.m)
Deflection (mm)
0
10
20
30
40
50
60
70
80
0
20
40
60
80
2T10B
ACI440 (2T10B)
CSA (2T10B)
2T20B
ACI440 (2T20B)
CSA (2T20B)

(d)

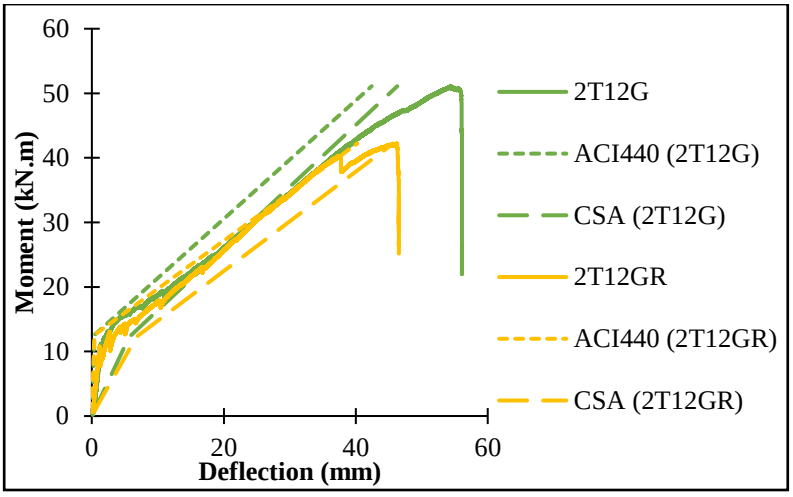

(e)

Figure 4-16: Analytical and experimental moment vs midspan deflection for (a) under-reinforced beams; (b) over-reinforced beams; (c) different number of bars; (d) BFRP reinforced beams; (e) different surface textures.

Table 4-5 lists the experimental and analytical deflection values. As mentioned previously, the deflections in this study were considered at a service loading level of $0.3M_n$. According to the ACI 440 code, the midspan deflection limit at the service loading level is the clear span length /240, which yields a value of 7.9 mm. It can be seen from Table 4-5 that all the FRP reinforced beams, except for 2T20G, satisfied the deflection limit at $0.3M_n$. The 2T20G beam reported a slightly larger deflection value (8.08 mm) than the limit. Thus, this shows that UHSC beams reinforced with FRP bars yield acceptable deflection values at service loads.

The table also shows that the ACI significantly underestimated the deflection values at a loading level of $0.3M_n$, especially for under-reinforced specimens. On the contrary, the CSA provided high deflection values for the under-reinforced beams at $0.3M_n$, but the predicted values for the over-reinforced beams were reasonable and slightly over-estimated, except for beam 2T20G. Hence, both the equations should be modified to obtain more accurate deflection values at the service loads. Furthermore, the ACI and CSA codes underestimated the deflection values at M_n with an average experimental to predicted ratio of 1.39 and 1.17, respectively. Goldston et al. [36] found that the ACI code underestimated the midspan deflection of HSC and UHSC beams by an average of 22% at the ultimate load level, whereas the CSA code underestimated the midspan deflection by an average of 10%. This supports the findings in this study regarding the predicted deflection values.

Table 4-5: Experimental and predicted service deflections.

Beam	Measured deflection (mm)		$\delta_{exp}/\delta_{pre}$ ACI 440.1R		$\delta_{exp}/\delta_{pre}$ CAN/CSA S806	
	$0.3M_n$	M_n	$0.3M_n$	M_n	$0.3M_n$	M_n
2T8G	0.79	35.25	3.87	1.18	0.12	0.79
2T8G-D	0.70	32.63	4.01	1.63	0.12	0.92
2T10G	1.07	43.32	3.26	1.22	0.17	1.04
2T12G	4.26	55.82	1.14	1.32	0.41	1.21
2T16G	6.29	57.06	1.74	1.89	0.80	1.76
2T20G	8.08	38.51	1.82	1.53	1.13	1.45
3T8G	1.29	39.78	4.53	1.12	0.20	0.91
3T10G	6.29	43.56	2.21	1.23	0.74	1.12
3T10G-D	6.22	43.82	2.85	1.30	0.80	1.18
2T12GR	2.60	46.17	4.65	1.15	0.34	1.01
2T10B	1.29	46.40	5.08	1.57	0.22	1.21
2T20B	6.93	38.32	1.46	1.49	0.94	1.43
	Average		3.05	1.39	0.50	1.17
	Standard Deviation		1.31	0.23	0.34	0.26

Chapter 5. Conclusion

This research investigated the flexural performance of beams developed using UHSC and reinforced with FRP bars. The effect of reinforcement ratio, number of bars, and reinforcement type was examined. In addition, equations from the FRP design codes were verified through comparison with the experimental data. Based on the experimental findings, the following was concluded:

1- FRP reinforced beams exhibited a bilinear moment-deflection behavior, with a reduced post cracking stiffness. Increasing the reinforcement ratio increased the post cracking stiffness. Also, increasing the reinforcement ratio led to a nonproportional increase in the moment capacity of the GFRP-UHSC beams. The increase followed a similar trend to that of the ACI 440 equation for evaluating the moment capacity. However, increasing the reinforcement ratio had an insignificant effect on the cracking moment.

2- The UHSC-FRP beams designed as compression-controlled showed some amount of ductility prior to failure, whereas tension-controlled beams experienced a brittle failure. Furthermore, the moment capacity increased from 51.1 kN.m to 56.0 kN.m for the 2T12G and 2T16G beams, which shows that changing the failure mode from FRP rupture to concrete crushing did not lead to a significant increase in the moment capacity.

3- Beams with low FRP reinforcement ratios had large increases in the bar strains at cracking due to their poor energy absorption capacity.

4- All the FRP reinforced beams satisfied the deflection limit at a service load level of $0.3M_n$, except for beam 2T20G. At a service load of $0.3M_n$, increasing the ρ_f/ρ_{fb} ratio caused the midspan deflection to increase for GFRP-UHSC beams. HSC and NSC beams in previous studies followed a different trend, where the deflection values decreased with an increasing ρ_f/ρ_{fb} ratio. Hence, care must be taken when designing UHSC beams with higher reinforcement ratios to prevent large service deflections.

5- The steel reinforced beams had higher post cracking stiffnesses and ductility than the GFRP reinforced beams. The steel reinforced beams also had smaller midspan deflection values than their GFRP counterparts.

However, the GFRP reinforced beams reported up to 70.15% increase in the flexural capacity compared to steel reinforced beams due to the high tensile strength of GFRP bars.

6- The GFRP and BFRP reinforced beams showed quite similar flexural behavior in terms of moment versus deflection response, strain values, and cracking patterns. Thus, BFRP bars can be great alternatives to GFRP bars in flexural members.

7- The beam with sand-coated GFRP bars had a larger flexural capacity and better cracking response than the beam with ribbed GFRP bars. This can be attributed to the higher tensile strength and better bond properties of sand-coated GFRP bars as compared to ribbed ones.

8- The ACI 440 and CAN/CSA S806 codes provided acceptable results for the cracking moment of UHSC beams. On average, the ratio of experimental to predicted cracking moment was found to be 0.93 for the ACI 440 code and 0.96 for the CAN/CSA S806 code.

9- The ACI 440 equation for predicting the flexural capacity provided conservative results for the under-reinforced GFRP-UHSC beams, but yielded unconservative values for over-reinforced GFRP-UHSC beams, as well as beams with BFRP reinforcement. On average, the ratio of experimental to predicted flexural capacity for all the tested specimens was found to be 1.05±0.14.

10- In general, the ACI 440 and CAN/CSA S806 design codes underestimated the maximum midspan deflections of the FRP reinforced specimens, especially for the over-reinforced beams, as they did not consider the additional ductility gained by those beams. It was found that the ACI 440 and CAN/CSA S806 codes yielded an average experimental to predicted midspan deflections of 1.39 and 1.17, respectively, at the ultimate moment level.

References

[1] American Concrete Institute, “Guide for the design and construction of structural concrete reinforced with fiber-reinforced polymer (FRP) bars,” ACI 440.1R-15, ACI Committee 440, Farmington Hills, MI, USA, 2015.

[2] Canadian Standard Association, “Design and construction of building structures with fibre-reinforced polymers,” CSA-S806-12, Mississauga, Ontario, Canada, 2012.

[3] F. Abed, M. Al-Mimar, and S. Ahmed, “Performance of BFRP RC beams using high strength concrete,” *Composites Part C: Open Access*, vol. 4, p. 100107, 2021, doi: 10.1016/j.jcomc.2021.100107.

[4] A. El-Nemr, E. A. Ahmed, and B. Benmokrane, “Flexural behavior and serviceability of normal- And high-strength concrete beams reinforced with glass fiber-reinforced polymer bars,” *ACI Structural Journal*, vol. 110, no. 6, pp. 1077-1088, 2013, doi: 10.14359/51686162.

[5] L. C. Bank. Composites for Construction. Hoboken, New Jersey: John Wiley & Sons, 2006, pp. 67-551.

[6] F. Elgabbas, E. A. Ahmed, and B. Benmokrane, "Physical and mechanical characteristics of new basalt-FRP bars for reinforcing concrete structures," *Construction and Building Materials*, vol. 95, pp. 623-635, 2015.

[7] S. Raj, V. R. Kumar, B. B. Kumar, and N. R. Iyer, "Basalt: structural insight as a construction material," *Sādhanā*, vol. 42, no. 1, pp. 75-84, 2017.

[8] S. Kocaoz, V. A. Samaranayake, and A. Nanni, “Tensile characterization of glass FRP bars,” *Composites Part B: Engineering*, vol. 36, no. 2, pp. 127-134, 2005, doi: 10.1016/j.compositesb.2004.05.004.

[9] F. Abed, Z. Mehaini, C. Oucif, A. Abdul-Latif, and R. Baleh, “Quasi-static and dynamic response of GFRP and BFRP bars under compression,” *Composites Part C: Open Access*, vol. 2, p. 100034, 2020, doi: 10.1016/j.jcomc.2020.100034.

[10] A. el Refai, F. Abed, and A. Altalmas, “Bond Durability of Basalt Fiber–Reinforced Polymer Bars Embedded in Concrete under Direct Pullout Conditions,” *Journal of Composites for Construction*, vol. 19, no. 5, p. 04014078, 2015, doi: 10.1061/(asce)cc.1943-5614.0000544.

[11] A. Altalmas, A. el Refai, and F. Abed, “Bond degradation of basalt fiber-reinforced polymer (BFRP) bars exposed to accelerated aging conditions,” *Construction and Building Materials*, vol. 81, pp. 162-171, 2015, doi: 10.1016/j.conbuildmat.2015.02.036.

[12] L. Hollaway, "The evolution of and the way forward for advanced polymer composites in the civil infrastructure," *Construction and Building Materials*, vol. 17, no. 6, pp. 365-378, Sep. 2003.

[13] "Ultra-High Performance Concrete", *Cement.org*, 2022. [Online]. Available: https://www.cement.org/learn/concrete-technology/concrete-design-production/ultra-high-performance-concrete. [Accessed: 05- Apr- 2022].

[14] N. Elmesalami, F. Abed, and A. el Refai, "Concrete Columns Reinforced with GFRP and BFRP Bars under Concentric and Eccentric Loads: Experimental Testing and Analytical Investigation," *Journal of Composites for Construction*, vol. 25, no. 2, p. 04021003, 2021, doi: 10.1061/(asce)cc.1943-5614.0001115.

[15] L. Alnajmi and F. Abed, "Evaluation of FRP bars under compression and their performance in RC columns," *Materials*, vol. 13, no. 20, p. 4541, 2020, doi: 10.3390/ma13204541.

[16] A. el Refai and F. Abed, "Concrete Contribution to Shear Strength of Beams Reinforced with Basalt Fiber-Reinforced Bars," *Journal of Composites for Construction*, vol. 20, no. 4, p. 04015082, 2016, doi: 10.1061/(asce)cc.1943-5614.0000648.

[17] F. Abed, M. K. Sabbagh, and A. S. Karzad, "Effect of basalt microfibers on the shear response of short concrete beams reinforced with BFRP bars," *Composite Structures*, vol. 269, p. 114029, 2021, doi: 10.1016/j.compstruct.2021.114029.

[18] F. Abed, A. el Refai, and S. Abdalla, "Experimental and finite element investigation of the shear performance of BFRP-RC short beams," *Structures*, vol. 20, pp. 689-701, 2019, doi: 10.1016/j.istruc.2019.06.019.

[19] A. El-Nemr, E. A. Ahmed, A. El-Safty, and B. Benmokrane, "Evaluation of the flexural strength and serviceability of concrete beams reinforced with different types of GFRP bars," *Engineering Structures*, vol. 173, pp. 606-619, 2018, doi: 10.1016/j.engstruct.2018.06.089.

[20] M. Chellapandian, A. Mani, and S. Suriya Prakash, "Effect of macro-synthetic structural fibers on the flexural behavior of concrete beams reinforced with different ratios of GFRP bars," *Composite Structures*, vol. 254, p. 112790, 2020, doi: 10.1016/j.compstruct.2020.112790.

[21] F. Elgabbas, P. Vincent, E. A. Ahmed, and B. Benmokrane, "Experimental testing of basalt-fiber-reinforced polymer bars in concrete beams," *Composites Part B: Engineering*, vol. 91, pp. 205-218, 2016, doi: 10.1016/j.compositesb.2016.01.045.

[22] F. Abed and A. R. Alhafiz, "Effect of basalt fibers on the flexural behavior of concrete beams reinforced with BFRP bars," *Composite Structures*, vol. 215, pp. 23-34, 2019, doi: 10.1016/j.compstruct.2019.02.050.

[23] A. el Refai, F. Abed, and A. Al-Rahmani, "Structural performance and serviceability of concrete beams reinforced with hybrid (GFRP and steel) bars," *Construction and Building Materials*, vol. 96, pp. 518-529, 2015, doi: 10.1016/j.conbuildmat.2015.08.063.

[24] H. Alkhraisha, H. Mhanna, N. Tello, and F. Abed, "Serviceability and flexural behavior of concrete beams reinforced with basalt fiber-reinforced polymer

(BFRP) bars exposed to harsh conditions," *Polymers (Basel)*, vol. 12, no. 9, p. 2110, 2020, doi: 10.3390/POLYM12092110.

[25] M. A. Adam, M. Said, A. A. Mahmoud, and A. S. Shanour, "Analytical and experimental flexural behavior of concrete beams reinforced with glass fiber reinforced polymers bars," *Construction and Building Materials*, vol. 84, pp. 354-366, 2015, doi: 10.1016/j.conbuildmat.2015.03.057.

[26] M. Thériault and B. Benmokrane, "Effects of FRP Reinforcement Ratio and Concrete Strength on Flexural Behavior of Concrete Beams," *Journal of Composites for Construction*, vol. 2, no. 1, pp. 7-16, 1998, doi: 10.1061/(asce)1090-0268(1998)2:1(7).

[27] O. I. Abdelkarim, E. A. Ahmed, H. M. Mohamed, and B. Benmokrane, "Flexural strength and serviceability evaluation of concrete beams reinforced with deformed GFRP bars," *Engineering Structures*, vol. 186, pp. 282-296, 2019, doi: 10.1016/j.engstruct.2019.02.024.

[28] J. M. Yang, K. H. Min, H. O. Shin, and Y. S. Yoon, "Effect of steel and synthetic fibers on flexural behavior of high-strength concrete beams reinforced with FRP bars," *Composites Part B: Engineering*, vol. 43, no. 3, pp. 1077-1086, 2012, doi: 10.1016/j.compositesb.2012.01.044.

[29] S. V. M. Esfahani and M. K. Sharbatdar, "Substitution effects of conventional concrete with high-performance fiber-reinforced cementitious composite (HPFRCC) in beams reinforced with GFRP bars," *Case Studies in Construction Materials*, vol. 13, p. e00440, 2020, doi: 10.1016/j.cscm.2020.e00440.

[30] M. A. Rashid, M. A. Mansur, and P. Paramasivam, "Behavior of aramid fiber-reinforced polymer reinforced high strength concrete beams under bending," *Journal of Composites for Construction*, vol. 9, no. 2, pp. 117-127, 2005.

[31] H. Zhu, S. Cheng, D. Gao, S. M. Neaz, and C. Li, "Flexural behavior of partially fiber-reinforced high-strength concrete beams reinforced with FRP bars," *Construction and Building Materials*, vol. 161, pp. 587-597, 2018, doi: 10.1016/j.conbuildmat.2017.12.003.

[32] M. S. Moawad and A. Fawzi, "Performance of concrete beams partially/fully reinforced with glass fiber polymer bars," *Journal of Engineering and Applied Science*, vol. 68, no. 1, pp. 1-18, 2021, doi: 10.1186/s44147-021-00028-6.

[33] L. Yinghao and Y. Yong, "Arrangement of hybrid rebars on flexural behavior of HSC beams," *Composites Part B: Engineering*, vol. 45, no. 1, pp. 22-31, 2013, doi: 10.1016/j.compositesb.2012.08.023.

[34] A. M. Erfan, H. E. Hassan, K. M. Hatab, and T. A. El-Sayed, "The flexural behavior of nano concrete and high strength concrete using GFRP," *Construction and Building Materials*, vol. 247, p. 118664, 2020, doi: 10.1016/j.conbuildmat.2020.118664.

[35] T. Wu, Y. Sun, X. Liu, and H. Wei, "Flexural Behavior of Steel Fiber–Reinforced Lightweight Aggregate Concrete Beams Reinforced with Glass Fiber–Reinforced Polymer Bars," *Journal of Composites for Construction*,

vol. 23, no. 2, p. 04018081, Apr. 2019, doi: 10.1061/(asce)cc.1943-5614.0000920.

[36] M. W. Goldston, A. Remennikov, and M. N. Sheikh, "Flexural behaviour of GFRP reinforced high strength and ultra high strength concrete beams," *Construction and Building Materials*, vol. 131, pp. 606-617, 2017, doi: 10.1016/j.conbuildmat.2016.11.094.

[37] D. Y. Yoo, N. Banthia, and Y. S. Yoon, "Predicting service deflection of ultra-high-performance fiber-reinforced concrete beams reinforced with GFRP bars," *Composites Part B: Engineering*, vol. 99, pp. 381-397, 2016, doi: 10.1016/j.compositesb.2016.06.013.

[38] D. Y. Yoo, N. Banthia, and Y. S. Yoon, "Flexural behavior of ultra-high-performance fiber-reinforced concrete beams reinforced with GFRP and steel rebars," *Engineering Structures*, vol. 111, pp. 246-262, 2016, doi: 10.1016/j.engstruct.2015.12.003.

[39] E. Ferrier, L. Michel, B. Zuber, and G. Chanvillard, "Mechanical behaviour of ultra-high-performance short-fibre-reinforced concrete beams with internal fibre reinforced polymer bars," *Composites Part B: Engineering*, vol. 68, pp. 246-258, 2015, doi: 10.1016/j.compositesb.2014.08.001.

[40] American Concrete Institute, "Building code requirements for structural concrete and commentary," ACI 318-19, Farmington Hills, MI, USA, 2019.

[41] American Concrete Institute, "Guide test methods for fibre-reinforced polymers (FRPs) for reinforcing or strengthening concrete structures," ACI 440.3R-12, ACI Committee 440, Farmington Hills, MI, USA, 2012.

[42] R. B. Khadiranaikar and M. M. Awati, "Concrete Stress Distribution Factors for High-Performance Concrete," *Journal of Structural Engineering*, vol. 138, no. 3, pp. 402-415, 2012, doi: 10.1061/(asce)st.1943-541x.0000465.

Vita

Zin Mahaini was born in 1998, in Damascus, Syria. She received her high school diploma from Al Maarifa International School, class of 2015. She was awarded her B.Sc. degree in Civil Engineering from the American University of Sharjah (AUS) in 2019. In February 2020, she joined the Civil Engineering Master's program in AUS as a graduate teaching and research assistant.